

Information for “The Contribution of Glacial Isostatic  
Adjustment to Projections of Sea Level Change Along the  
Atlantic and Gulf coasts of North America”

Ryan Love<sup>1</sup>, Glenn A. Milne<sup>2</sup>, Lev Tarasov<sup>3</sup>, Simon E. Engelhart<sup>4</sup>, Marc P. Hijma<sup>5</sup>,  
Konstantin Latychev<sup>6</sup>, Benjamin P. Horton<sup>7</sup>, and Torbjörn E. Törnqvist<sup>8</sup>

<sup>1</sup> *Department of Physics, University of Ottawa, Present address: Department of Physics and Physical  
Oceanography, Memorial University of Newfoundland,*

<sup>2</sup> *Department of Earth and Environmental Sciences, University of Ottawa, Ottawa, Ontario*

<sup>3</sup> *Department of Physics and Physical Oceanography, Memorial University of Newfoundland*

<sup>4</sup> *Department of Geosciences, The University of Rhode Island*

<sup>5</sup> *Department of Earth and Environmental Sciences, Tulane University, New Orleans, LA, USA, Present  
address: Department of Applied Geology and Geophysics, Delft, The Netherlands*

<sup>6</sup> *Department of Physics, University of Toronto, Toronto*

<sup>7</sup> *Department of Sea Level Research, Department of Marine and Coastal Sciences, Rutgers, New Brunswick,  
New Jersey, USA; Earth Observatory of Singapore, Asian School of the Environment, Nanyang Technological  
University, 639798, Singapore*

<sup>8</sup> *Department of Earth and Environmental Sciences, Tulane University, New Orleans, LA, USA*

# 1 Finite Volume (3D) Earth Model

In order to determine lateral changes in mantle viscosity from a model of seismic wave velocities we utilize the following relationships

$$\delta \ln \rho(r, \theta, \phi) = \left( \frac{\partial \ln \rho}{\partial \ln v_s}(r) \right) \delta \ln v_s(r, \theta, \phi), \quad (1)$$

$$\delta T(r, \theta, \phi) = -\frac{1}{\alpha(r)} \delta \ln \rho(r, \theta, \phi), \quad (2)$$

$$\nu(r, \theta, \phi) = \nu_0(r) e^{\epsilon \delta T(r, \theta, \phi)}, \quad (3)$$

where  $r, \theta, \phi$  are the usual spherical co-ordinates,  $\rho$  is the density,  $v_s$  is the velocity of shear waves,  $T$  is the temperature,  $\alpha$  is the coefficient of thermal expansion,  $\epsilon$  is a control parameter,  $\nu$  and  $\nu_0$  are, respectively, the viscosity we determine and the viscosity of the background model. The control parameter is used such that if a value of zero is prescribed no lateral viscosity structure is applied and only the 1D background viscosity structure is implemented. When  $\epsilon$  is non-zero, the 3D viscosity structure is adjusted such that the global average of the viscosity of any given layer matches the prescribed 1D viscosity profile. We obtain  $\delta \ln v_s(r, \theta, \phi)$  from the S40RTS model of *Ritsema et al.* (2011) and we utilize the same layered structure that is used in the 1D spherically symmetric model for our background viscosity model. We chose to use the same depth layering such that the differences between the 1D and 3D models is due only to the existence of lateral structure. For full details regarding the finite volume implementation of the related glacial isostatic adjustment (GIA) response theory see *Latychev et al.* (2005).

To examine the influence of lateral Earth structure we utilize a control case where the 3D model has the same depth-averaged Earth structure and ice loading history as one of the best-fitting 1D models (*Tarasov et al.* (2012), *Peltier* (2004), *Lecavalier et al.* (2014)), see main text. We note that the sea-level equation applied in the 3D Earth simulations is the same as that used for the 1D model and so includes time-varying shoreline position, although it does not contain the rotational feedback. As well, the resolution of the 3D model is  $\approx 20$ km laterally at the surface and decreases with depth. The results shown in Figure 4 (main text) and Supplementary Material (SM) Figure S13 show the difference between the output from the full 3D model relative to the chosen 1D control case. The computational run time of this particular model is significantly longer than the 1D model. A single model run using  $> 100$  processors in parallel takes  $\approx 6$  days and so the parameter space we can explore in a reasonable timespan is much smaller. Given the considerable uncertainty in defining lateral structure, results based on a single realization of this structure can only be considered preliminary. Sample depths from our single realization of 3D mantle viscosity are shown in SM Figures S1 to S3.

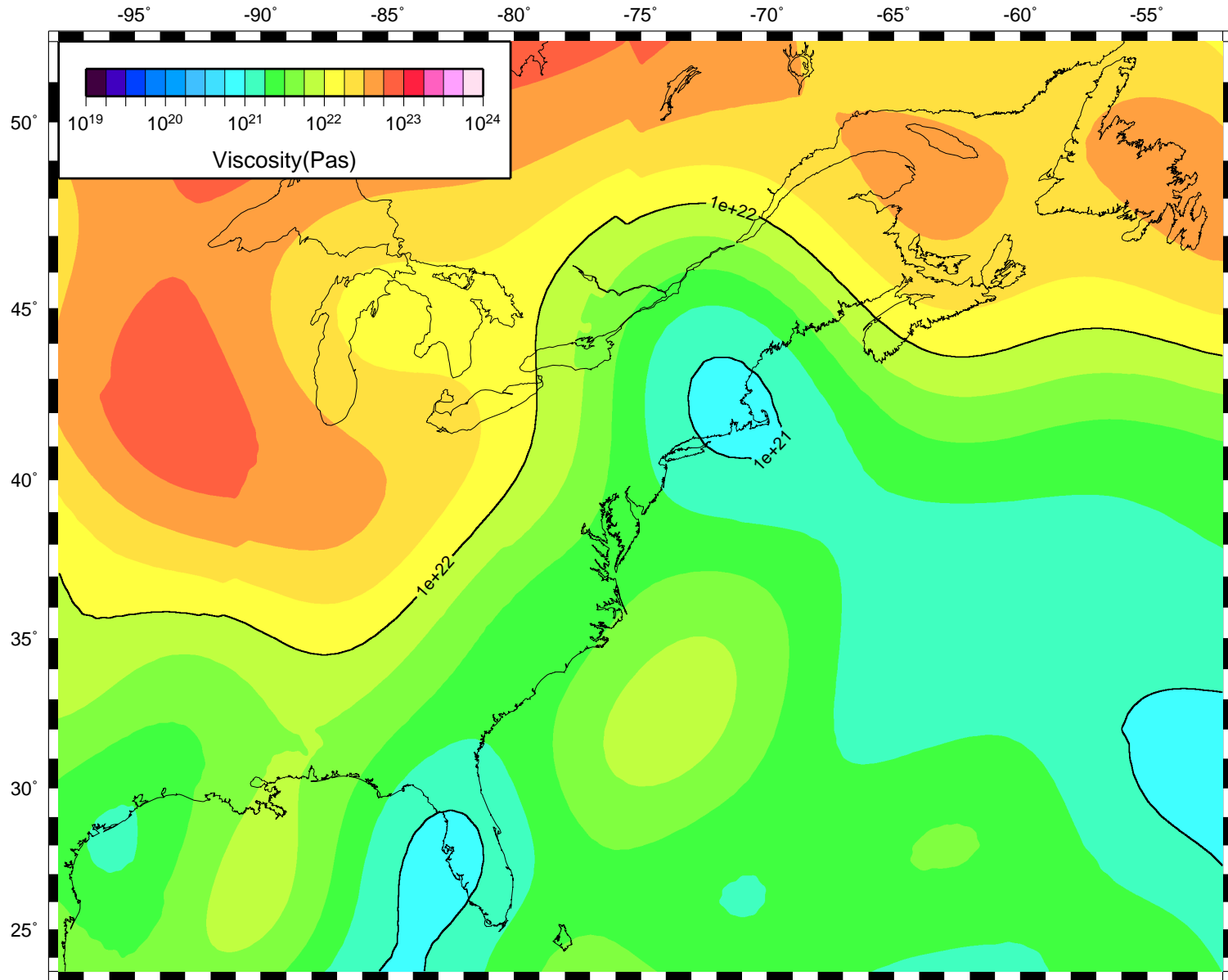


**Figure S1:** Mantle viscosity map for the study region at 220km depth from the surface. The lateral structure was determined using the global seismic velocity model S40RTS. The absolute values are scaled such that the global average viscosity value in is equal to that of the 1D viscosity model that produced an optimum fit for the entire RSL data base using the ice model 9894 (LT=71km, UMV= $3 \times 10^{21}$  Pas, LMV= $90 \times 10^{21}$  Pas).

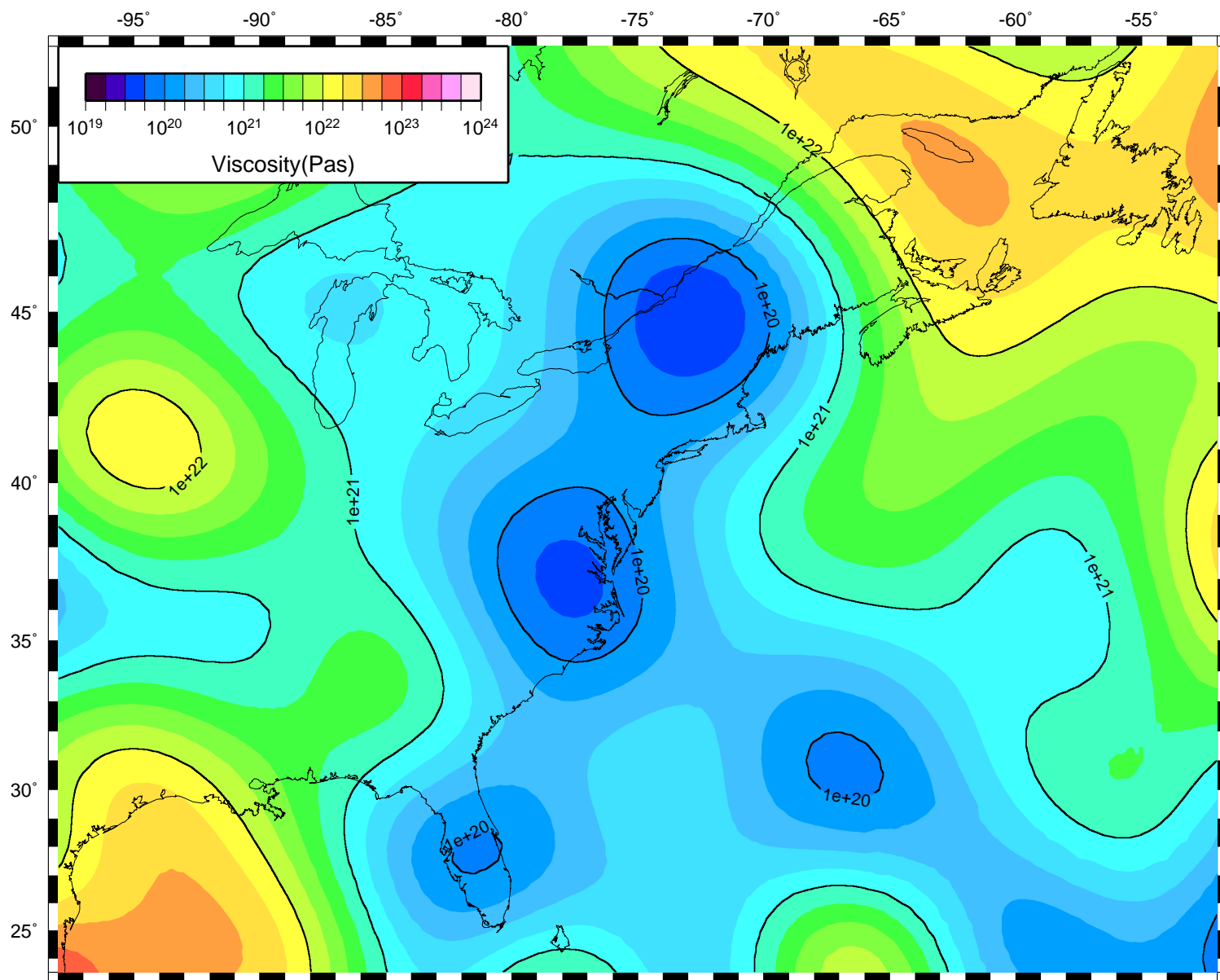


**Figure S2:** As for SM Figure S1 but for 551km depth.

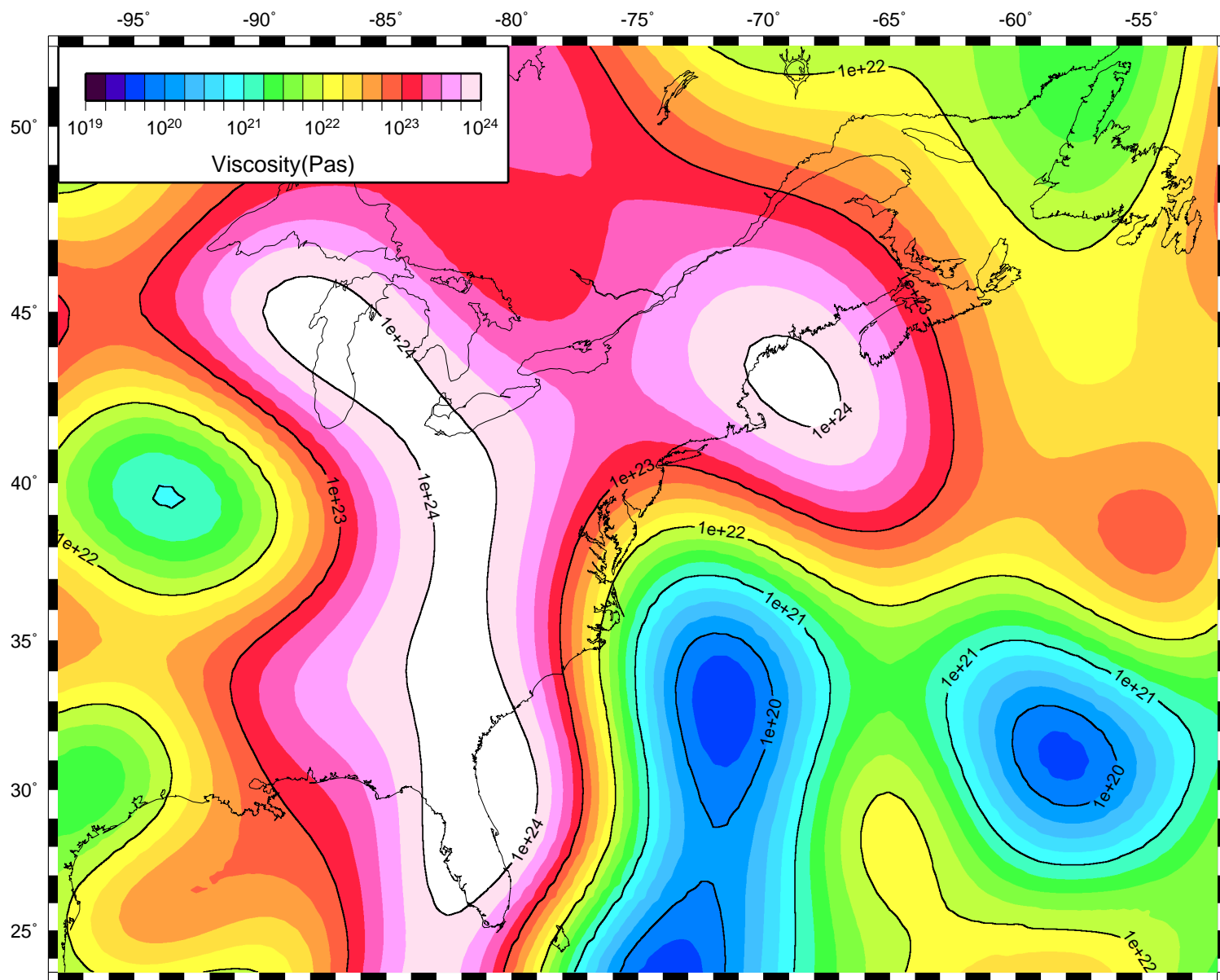


**Figure S3:** As for SM Figure S1 but for 1021km depth.

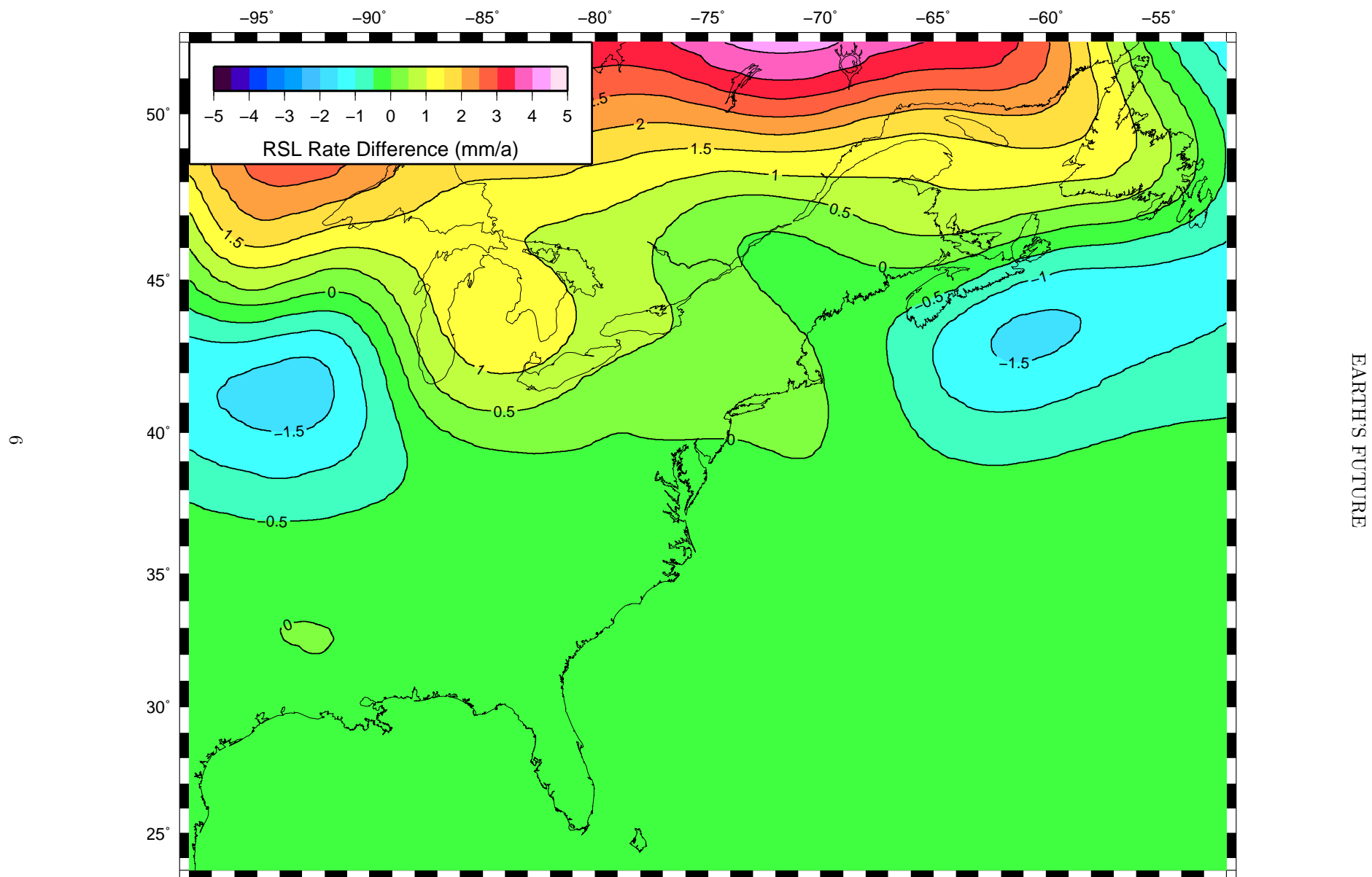


**Figure S4:** Difference in RSL rates (over the period 1000CE-2000CE) between the Locally Scaled model and the 1D equivalent 3D model run.

## 2 Glacial Systems Model

The 35 Glacial Systems Model (GSM) runs were selected from the large ensemble calibration results of *Tarasov et al.* (2012) to provide a high variance sub-ensemble over a range of weights for various metric components (including whole ice complex RSL and uplift fits, marine limit fits, and strandline fits, among others). Average and standard deviation maps from this ensemble at 21 ka BP and 10 ka BP are shown in SM Figures S5 to S8. Runs were first sieved according to constraints described in Table 1 of *Tarasov et al.* (2012). Five runs were selected based solely on overall metric fits for the whole ice sheet (4247, 5962, 6244, 9894, 9927). 9927 and 9894 are presented in detail in *Tarasov et al.* (2012).

The remaining reconstructions were selected by various combinations of increased weight to regional fits to RSL and present-day vertical velocity data (Southern Ontario to Newfoundland and south to US East Coast) as well as varying acceptance thresholds for general fits to strandline and marine limit data. Seven "extremal" chronologies (6317, 6318, 7042, 7221, 7239, 8025, 9085) were extracted to capture uncertainty bounds for various metric components and NAIC ice volume. As detailed in *Tarasov et al.* (2012), the GSM was run only with the VM5 earth model (*Peltier and Drummond* (2008)). The GSM, metric components, and ensemble calibration are described in *Tarasov et al.* (2012) and references therein.

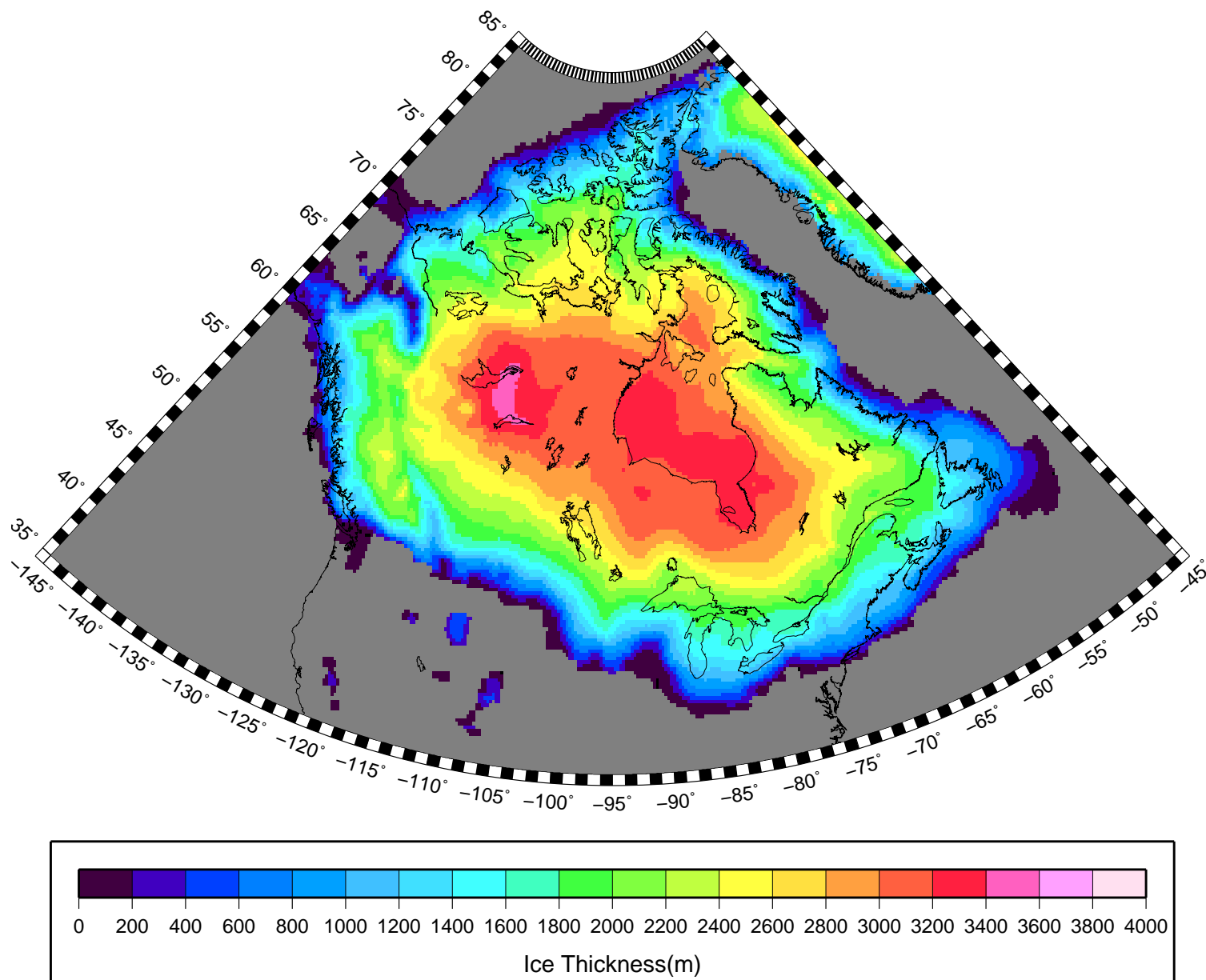


**Figure S5:** Average ice sheet thickness from our 35 model ensemble at 21 ka BP.



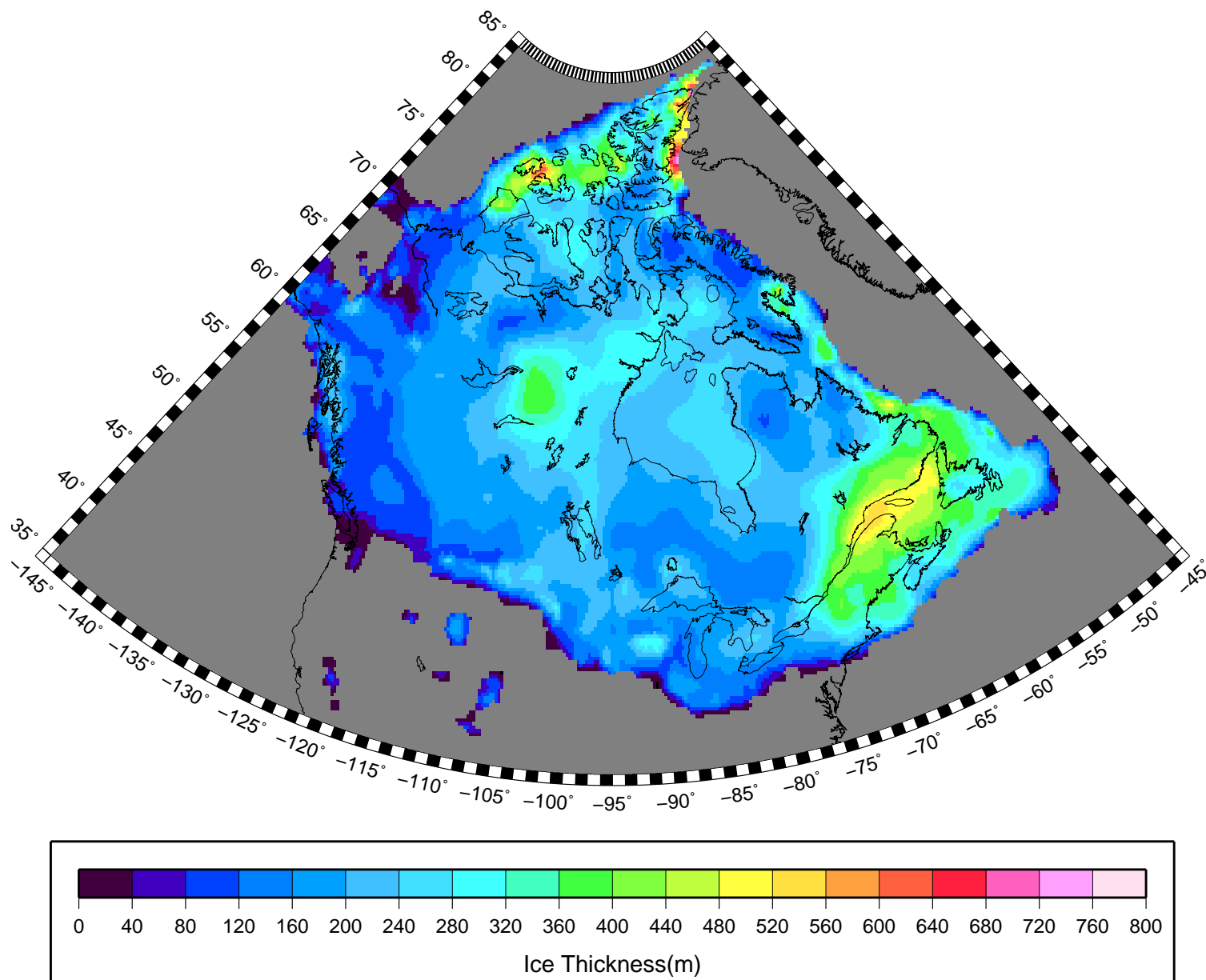


**Figure S6:** One standard deviation of ice sheet thickness for our 35 model ensemble at 21 ka BP.

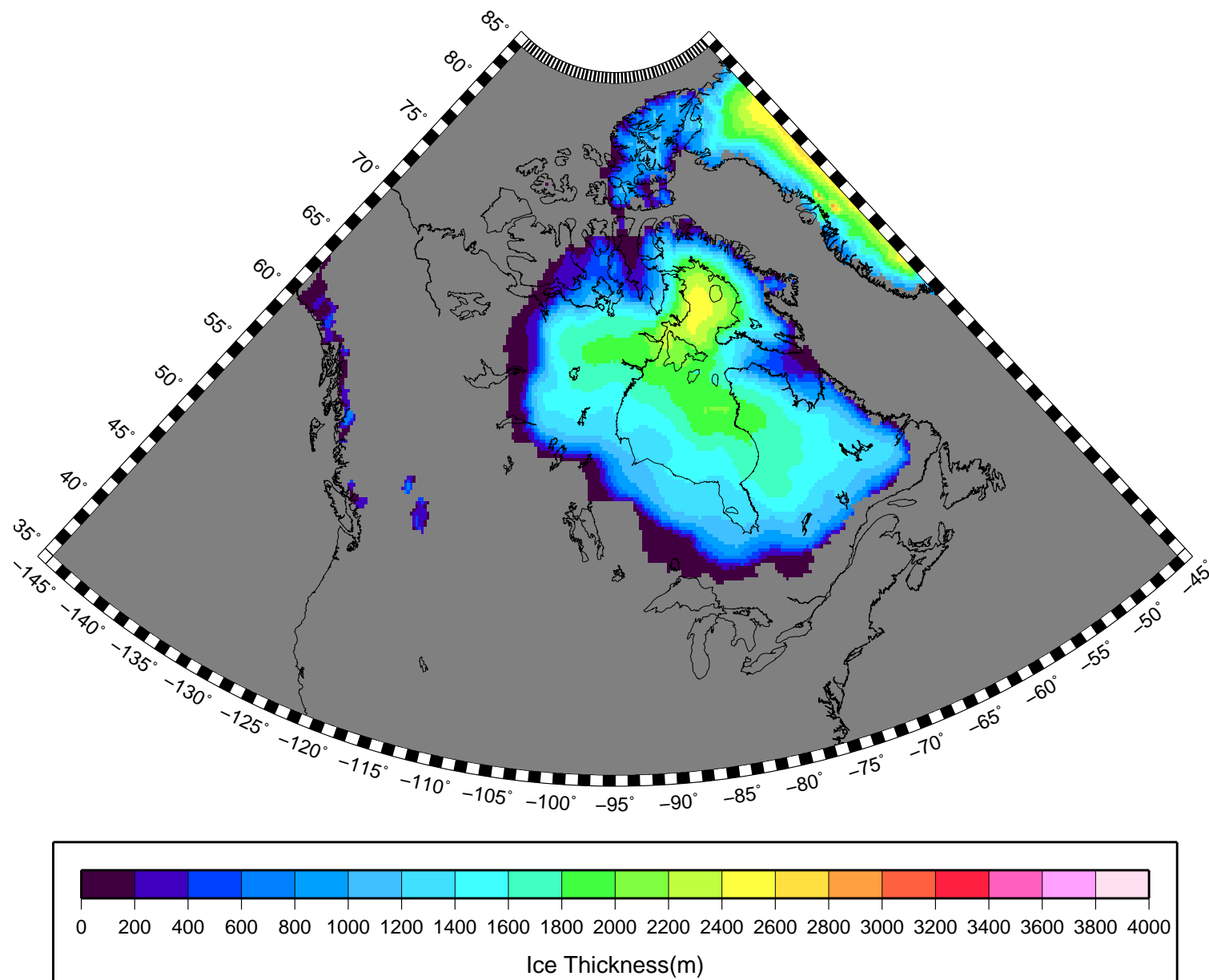


**Figure S7:** Average ice sheet thickness from our 35 model ensemble at 10 ka BP.

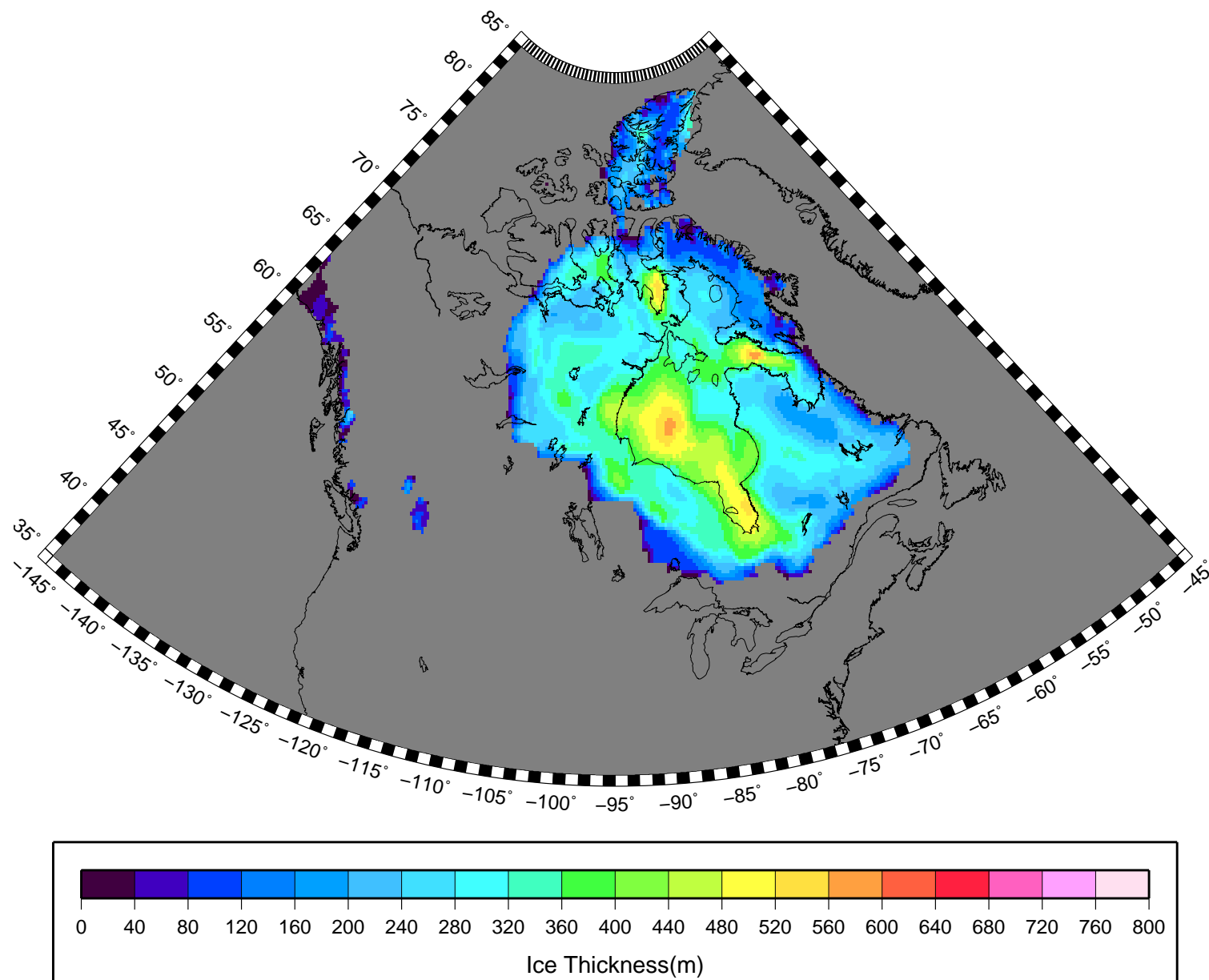


**Figure S8:** One standard deviation of ice sheet thickness for our 35 model ensemble at 10 ka BP.

### 3 RSL Data

The majority of the RSL data from the Atlantic Coast have been presented in an earlier publication (*Engelhart and Horton (2012)*), with the exception of the new data from Canada (37 index points). The United States (US) Gulf coast RSL database is newly presented in this paper and is a greatly expanded version of the database published by *Hijma et al. (2015)*. It extends from the Florida Keys to Texas and contains 291 SLIPs and 587 limiting data points. The complete Gulf coast database is plotted in SM Fig. S9, showing a relatively coherent trend of RSL rise across this large region due to the fact that differential GIA effects are small compared to those along the Atlantic Coast. Despite its greater distance from the NAIC, the overarching characteristic is that throughout the Gulf coast, there is no evidence for a Holocene highstand as RSL was always below present mean sea level over the past 12 ka.

The Gulf coast dataset is contained in an included spreadsheet (USGulfCoastRSLDatabase2015.ods), also the Canadian coast RSL dataset is contained in a separate spreadsheet (CanCoastRSLDatabase2015.ods). As well RSL projections data produced from the 1D RSL model is available in both a gridded format (NetCDF) as well as tabular format (sampled at the Permanent Service for Mean Sea Level (PSMSL) tide gauge locations along our coastlines of interest) in the data tarball which accompanies this document and which this document is part of.

As stated in the main text, SLIPs and limiting data in the Mississippi delta region were corrected for sedimentary isostatic adjustment. For samples taken between -92 and -89 degrees longitude a correction of 0.25 mm/a was used, while for the flanks of the delta (between -93.5 to 92 and between -89 to -87.5 degrees longitude) a correction of 0.1 mm/a was used (based on *Yu et al. (2012)*; *Wolstencroft et al. (2014)*).

The Gulf coast database was constructed according to the protocol detailed by *Hijma et al. (2015)* and includes, among others, a variety of corrections and errors associated with  $^{14}\text{C}$  dating and inclusion of uncertainties in the vertical dimension based on the *Hill et al. (2011)* paleotidal model. A summary version of this database is released here, which includes 11 variables for each location compared to 77 in the full version. The literature from which the SLIP information was compiled and assessed is provided in the reference list at the end of this document. The full database includes quantitative data (wherever available) on the position of samples with respect to the compaction-free substrate. We used this information to identify RSL-data that have experienced relatively little to no compaction. Specifically, in order to be considered compaction-free, samples had to satisfy one of the following three criteria:

1. The samples were taken at or less than 0.2 m above the consolidated substrate
2. If the depth to the consolidated substrate is no more than 0.2 m, but less than 3% of the total depth of the sample. This means that a sample that lies 20 m deep and 0.5 m above a consolidated substrate is included.
3. The samples come from a continuous peat layer resting directly on top of the consolidated substrate that extends to the modern surface. The samples were taken from a continuous core. In this case, the depth to the consolidated substrate is irrelevant.

The same criteria were followed in producing a subset of the US East Coast dataset that can be considered effectively compaction free.

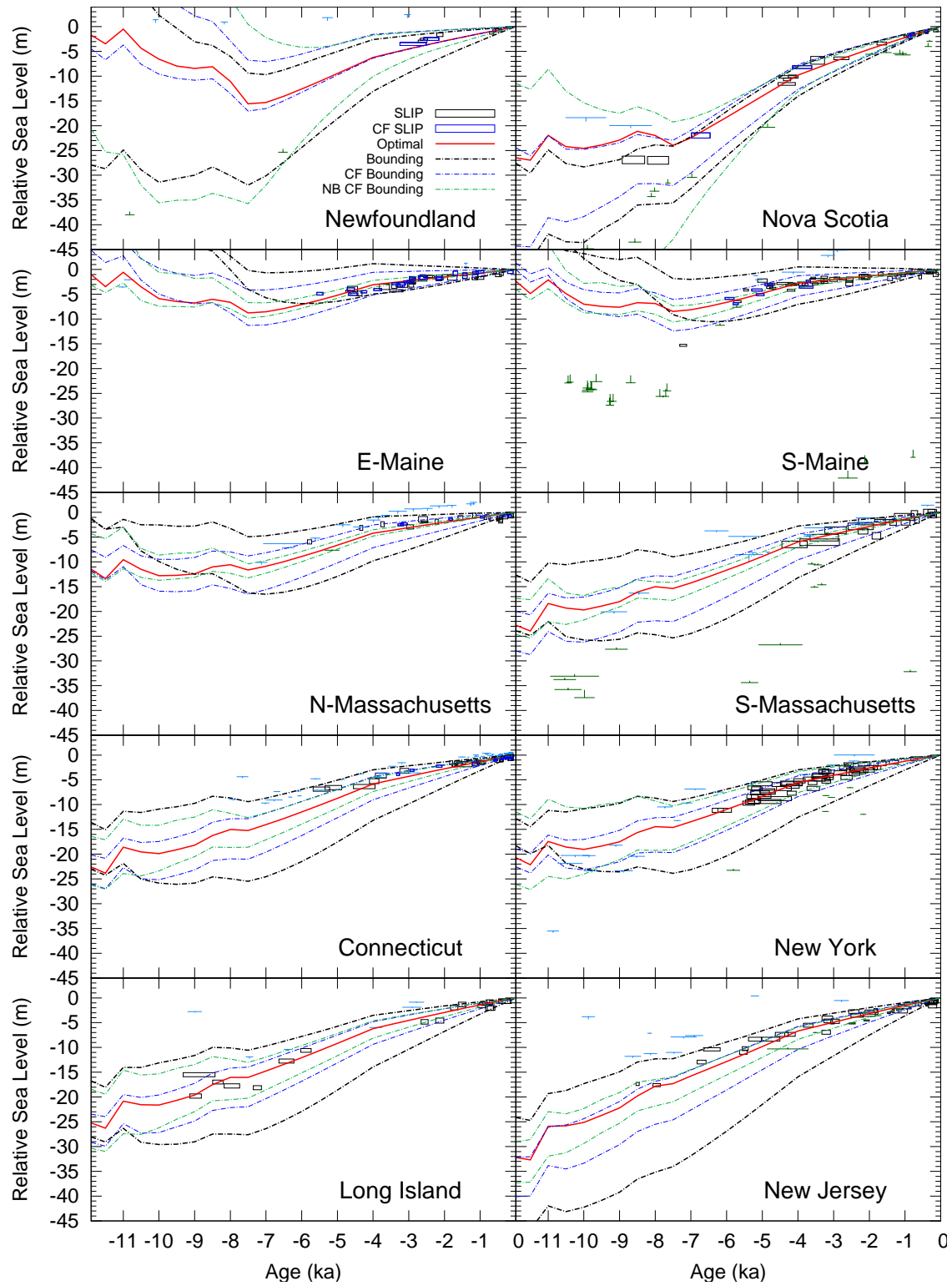


**Figure S9:** SLIPs for all sites along both the US East and Gulf coasts and indicated in Fig. 1, along with the optimal (best-fitting) model time series (red line). The SLIPs drawn in blue can be considered compaction free (indicated by 'CF SLIP' in key). Continued below;

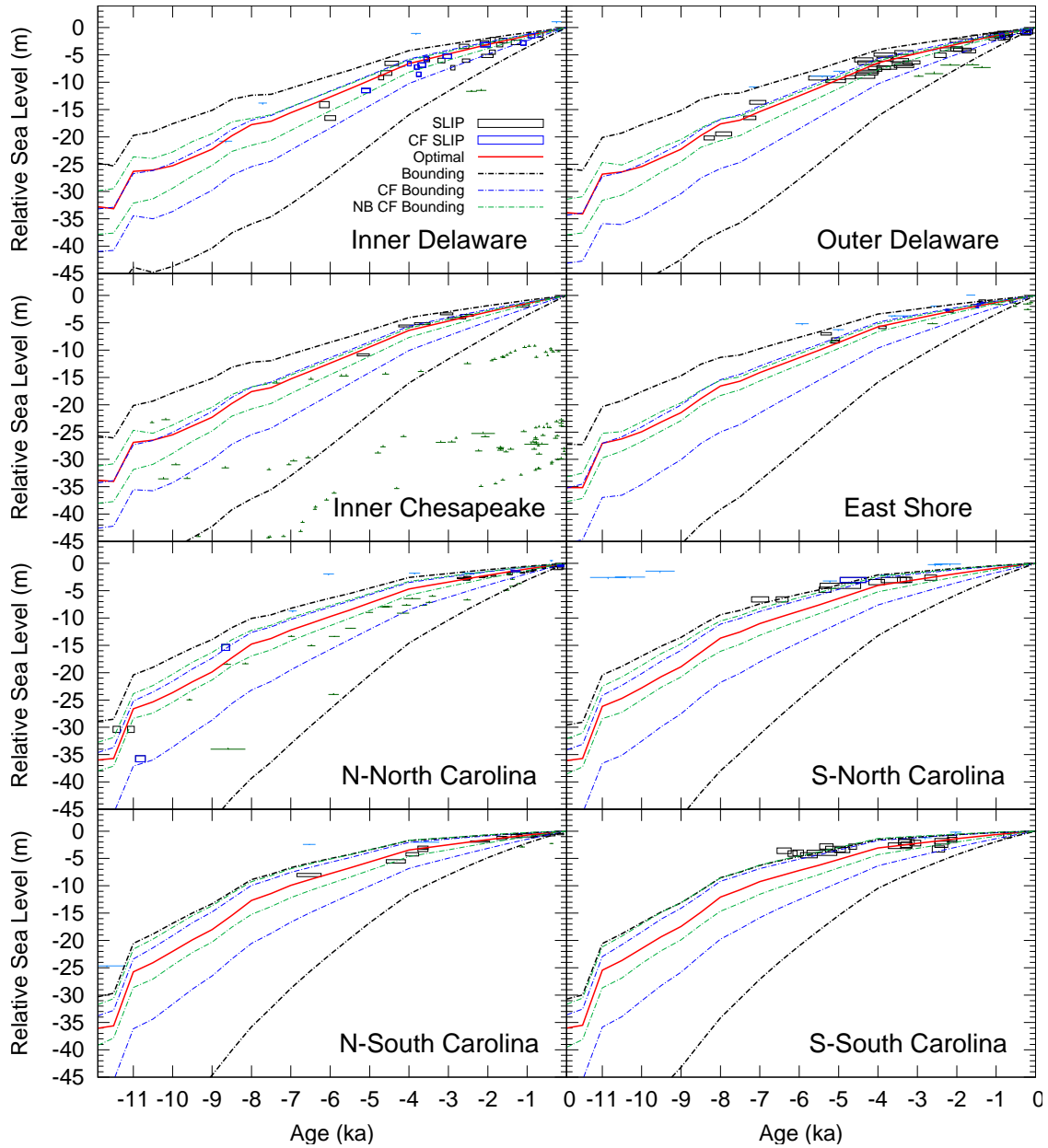


**Figure S9:** Continued from above; The dimensions of each SLIP box indicate the associated  $1\text{-}\sigma$  time and height uncertainties. We show these rather than the more conventional  $2\text{-}\sigma$  ranges because no bounding models were found using this more conservative range (see main text for details) and so the bounding runs (dash-dotted lines) represent  $1\text{-}\sigma$  uncertainty estimates. The black dash-dotted lines define the estimated  $1\text{-}\sigma$  bounds when all SLIPs in each sub-region are considered. The blue dash-dotted lines define the estimated  $1\text{-}\sigma$  bounds when only compaction free SLIPs in each sub-region are considered. The optimal run (red line) was determined using all the SLIPs in each sub-region. Limiting data are indicated by either green 'T' symbols (upper limiting) or blue inverted 'T' symbols (lower limiting). These were not used in estimating the optimal or bounding models but serve as a useful check on the accuracy of these model estimates (see text for further discussion). Note that all model curves (optimal and bounds) are generated at the locations indicated by white crosses in Fig. 1.

# EARTH'S FUTURE

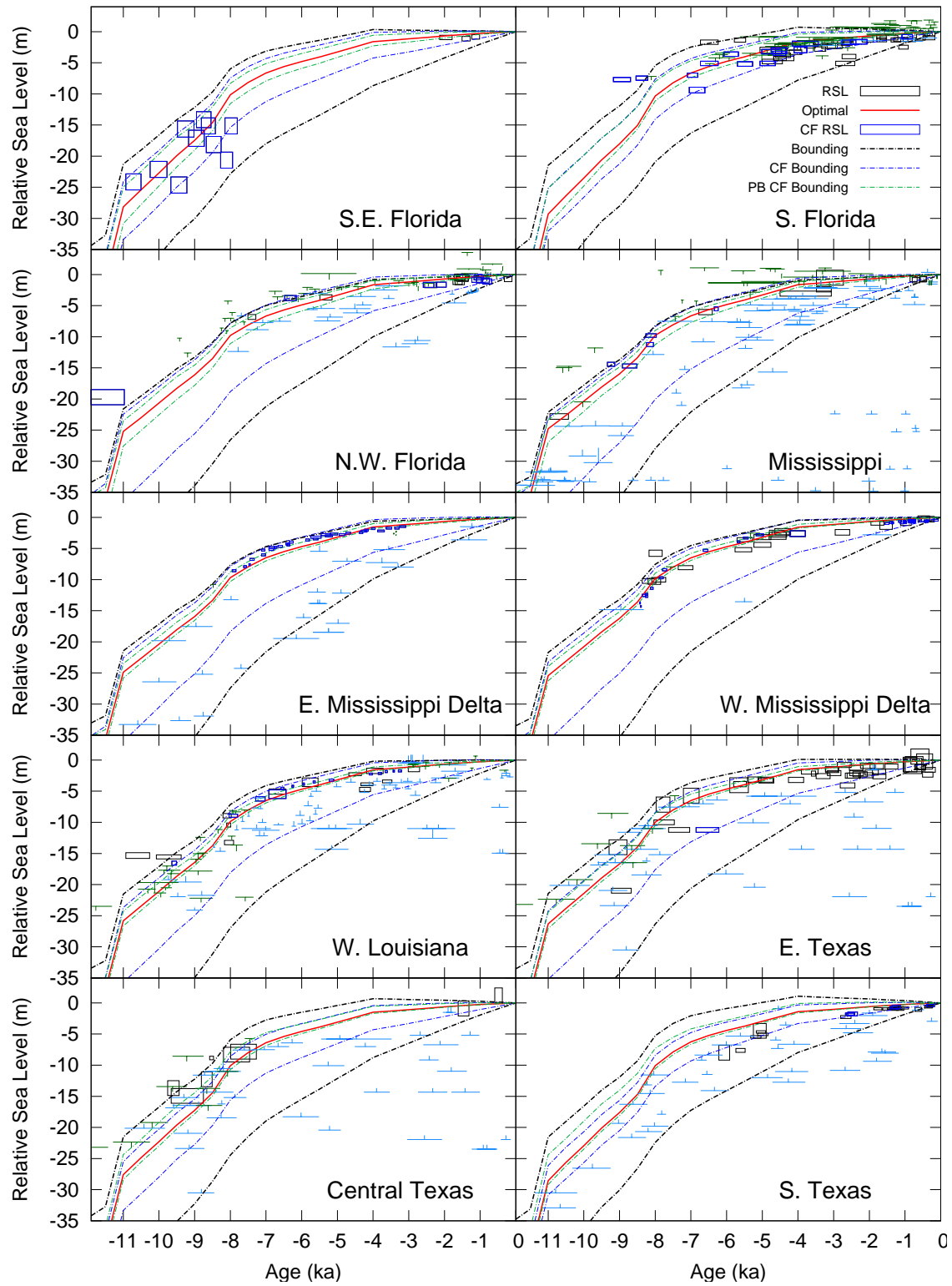


**Figure S9:** Continued from above

## 4 GIA model parameter estimation

Model parameter estimation is described in detail in Section 2.3.1 of the main text. The figures shown below (S10-S12) are referred to in the main text and so no additional information is provided here.



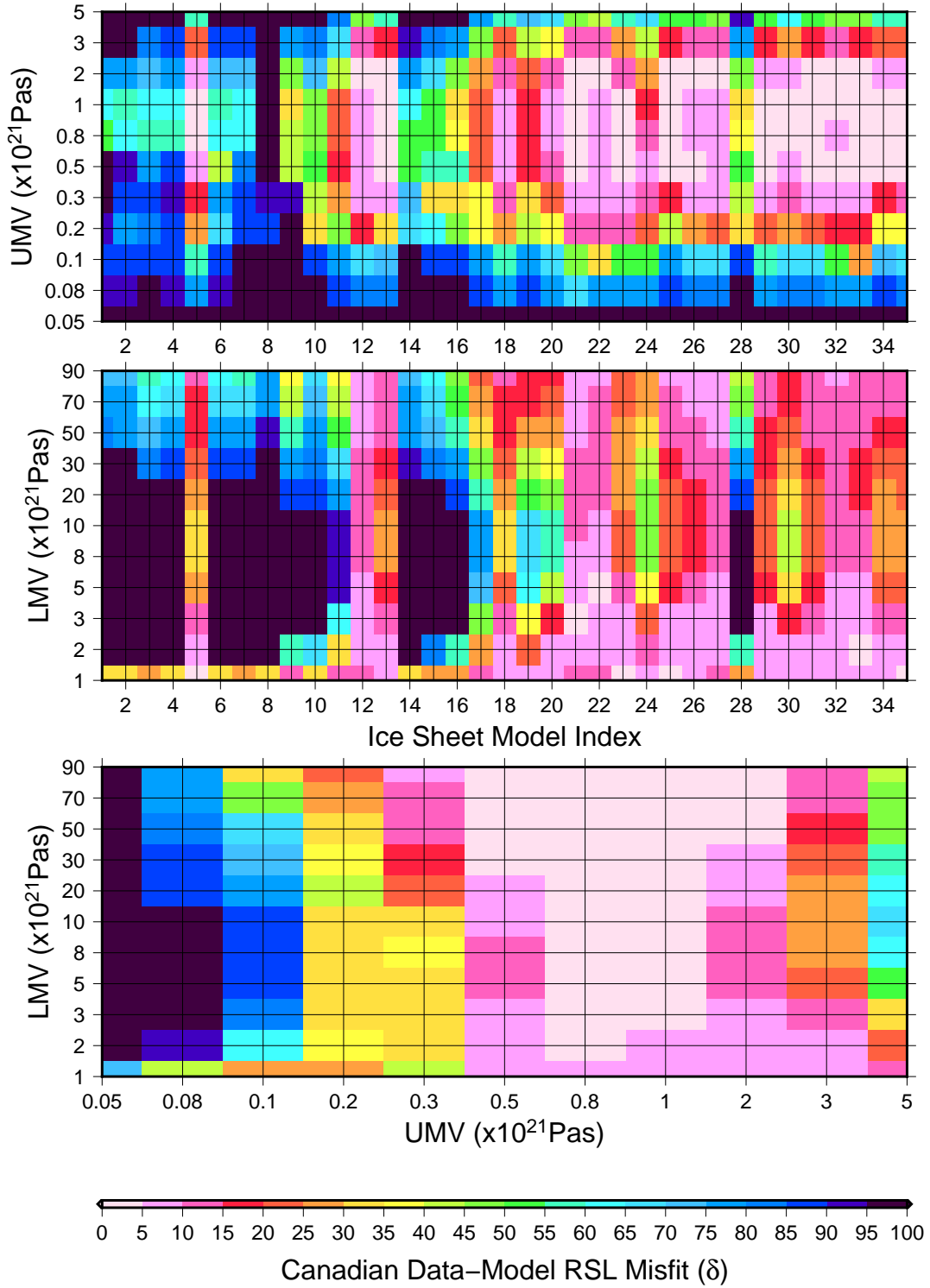


**Figure S10:** Data-model misfit plots for the Canadian dataset as a function of (from top to bottom) upper mantle viscosity and ice sheet model index (lower mantle constant at  $30 \times 10^{21}$  Pas), lower mantle viscosity and ice sheet model index (upper mantle viscosity constant at  $3 \times 10^{21}$  Pas), and upper mantle viscosity and lower mantle viscosity (ice sheet model index set to 34; 9894 ice history of *Tarasov et al.* (2012)). Lithospheric thickness is 71 km for all results shown.

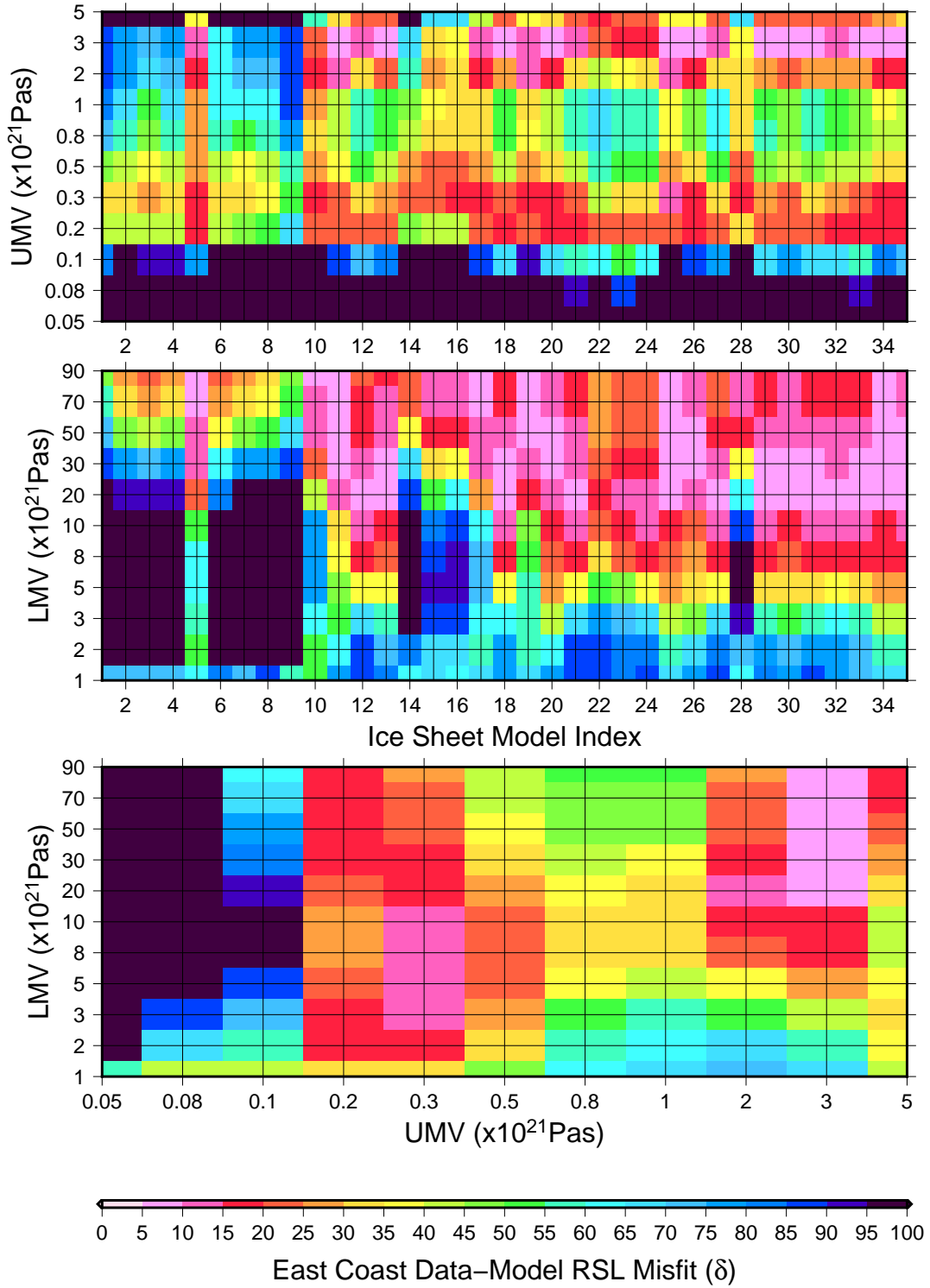


**Figure S11:** Data-model misfit plots for the US East coast dataset as a function of (from top to bottom) upper mantle viscosity and ice sheet model index (lower mantle constant at  $30 \times 10^{21}$  Pas), lower mantle viscosity and ice sheet model index (upper mantle viscosity constant at  $3 \times 10^{21}$  Pas), and upper mantle viscosity and lower mantle viscosity (ice sheet model index set to 34; 9894 ice history of *Tarasov et al.* (2012)). Lithospheric thickness is 71 km for all results shown.

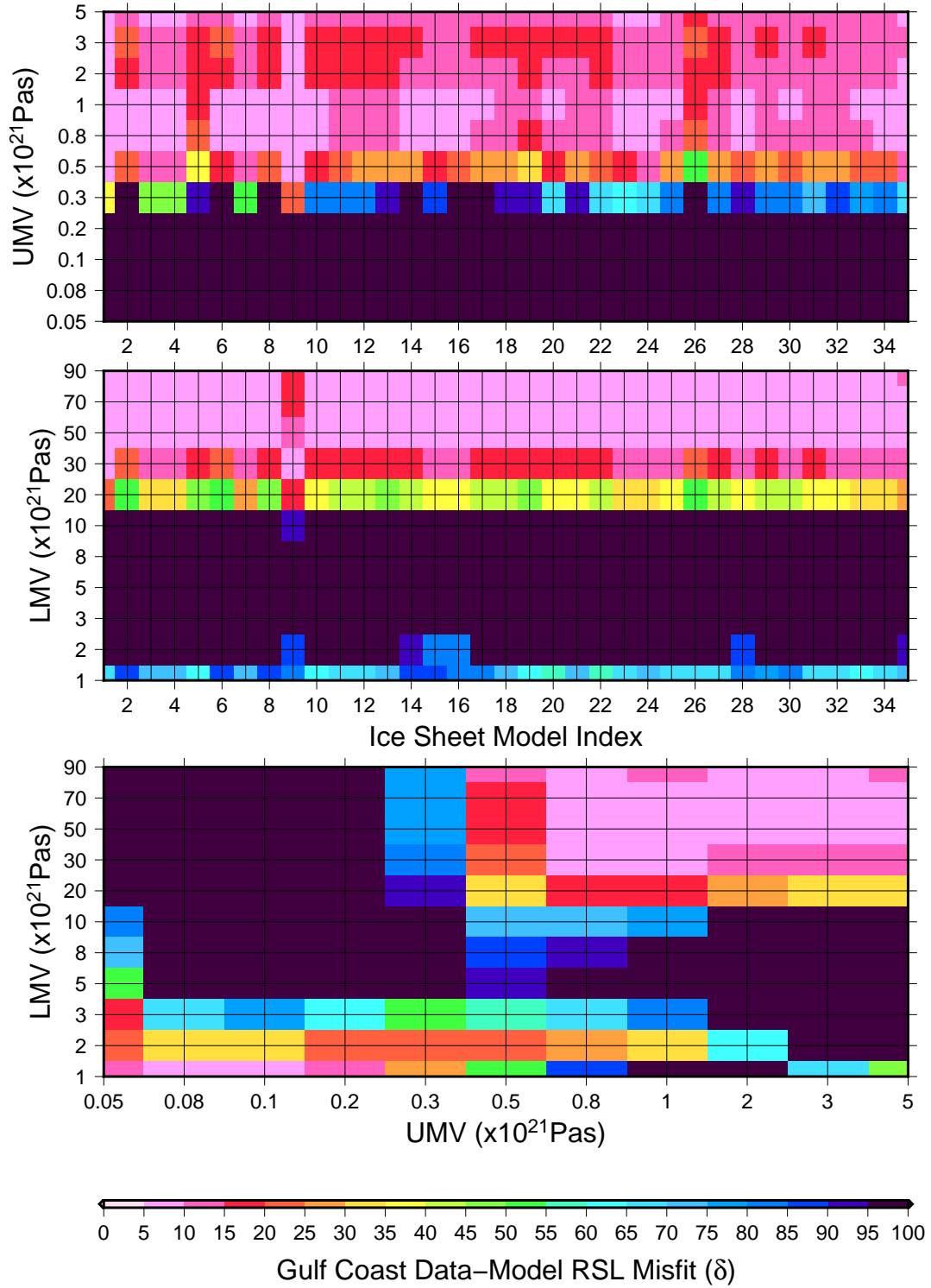


**Figure S12:** Data-model misfit plots for the Gulf coast dataset as a function of (from top to bottom) upper mantle viscosity and ice sheet model index (lower mantle constant at  $30 \times 10^{21}$  Pas), lower mantle viscosity and ice sheet model index (upper mantle viscosity constant at  $3 \times 10^{21}$  Pas), and upper mantle viscosity and lower mantle viscosity (ice sheet model index set to 34; 9894 ice history of *Tarasov et al.* (2012)). Lithospheric thickness is 71 km for all results shown.

Data Set	Model Run	LT (km)	UMV (x1021 Pas)	LMV (x1021 Pas)	ISMI
All	Optimal	71	3	90	5
CAC	Optimal	120	2	90	27
	Upper bound	96	1	70	22
	Lower bound	71	0.8	10	5
USAC	Optimal	71	3	30	34
	Upper bound	96	3	30	18
	Lower bound	120	5	70	16
USGC	Optimal	120	5	50	2
	Upper bound	120	0.1	90	33
	Lower bound	120	0.5	90	1
Compaction Free					
CAC	Upper bound	120	1	20	33
	Lower bound	71	0.8	10	23
USAC	Upper bound	120	1	20	29
	Lower bound	120	3	90	10
USGC	Upper bound	71	0.2	20	1
	Lower bound	96	1	70	4

**Table S1:** Model parameters for the optimal and bounding runs of the different regional datasets: Canada Atlantic coast (CAC), US Atlantic coast (USAC), US Gulf coast (USGC). Optimal model parameters also given for the complete dataset (indicated by 'All').

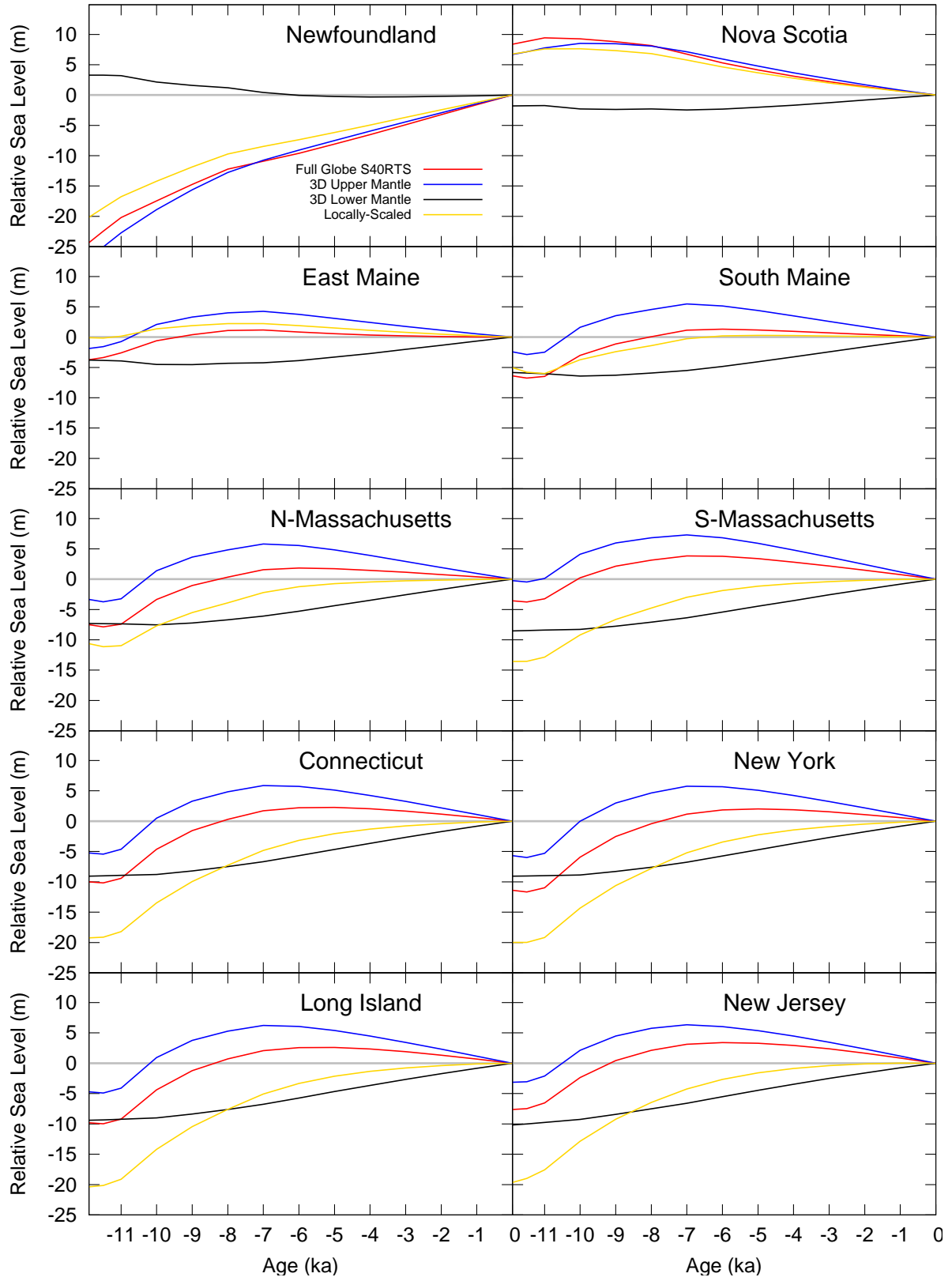


**Figure S13:** The influence of lateral Earth viscosity structure relative to the 1-D model control case for select locations. Results for all 28 localities (white crosses in Fig. 1) are shown.

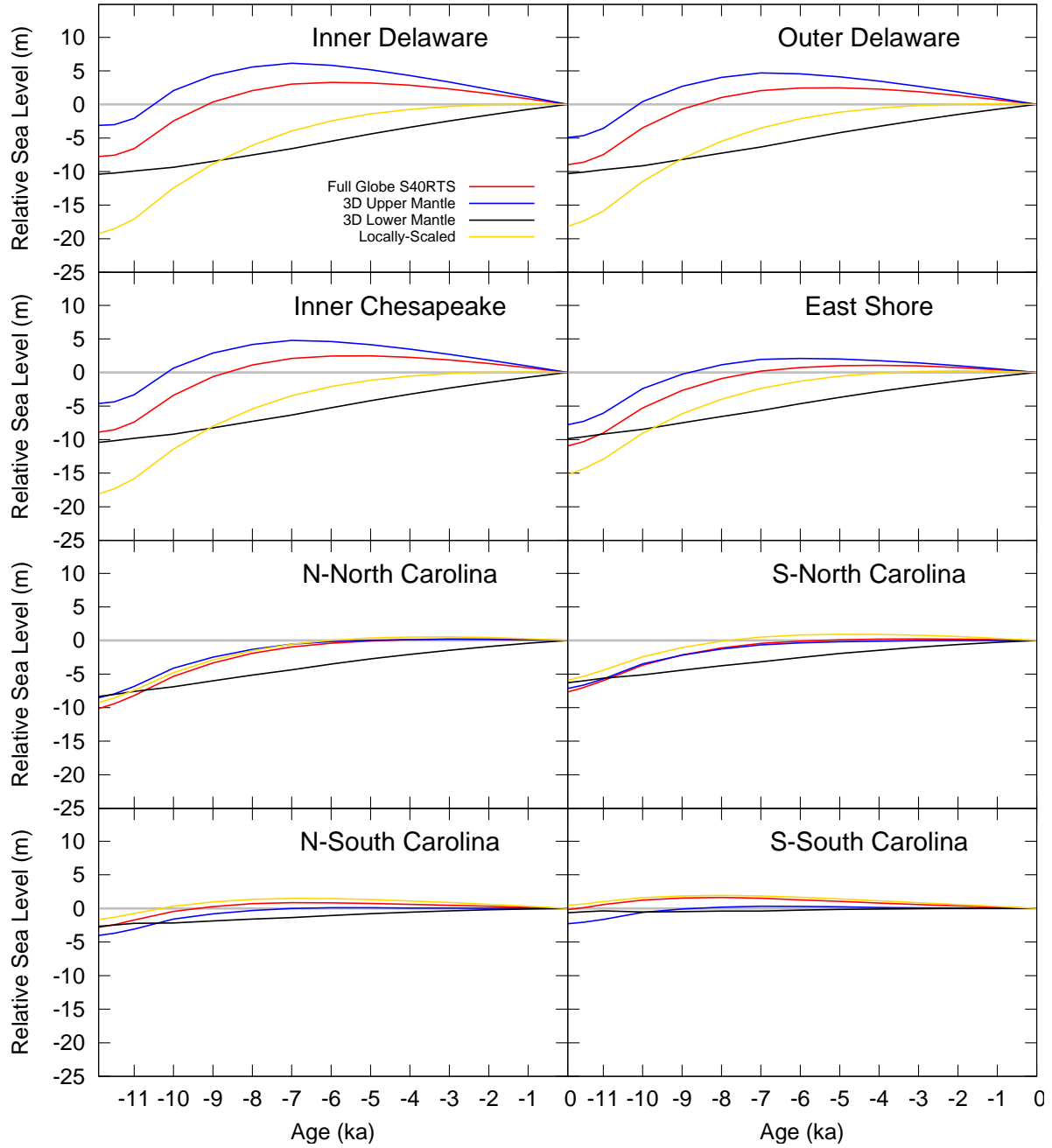
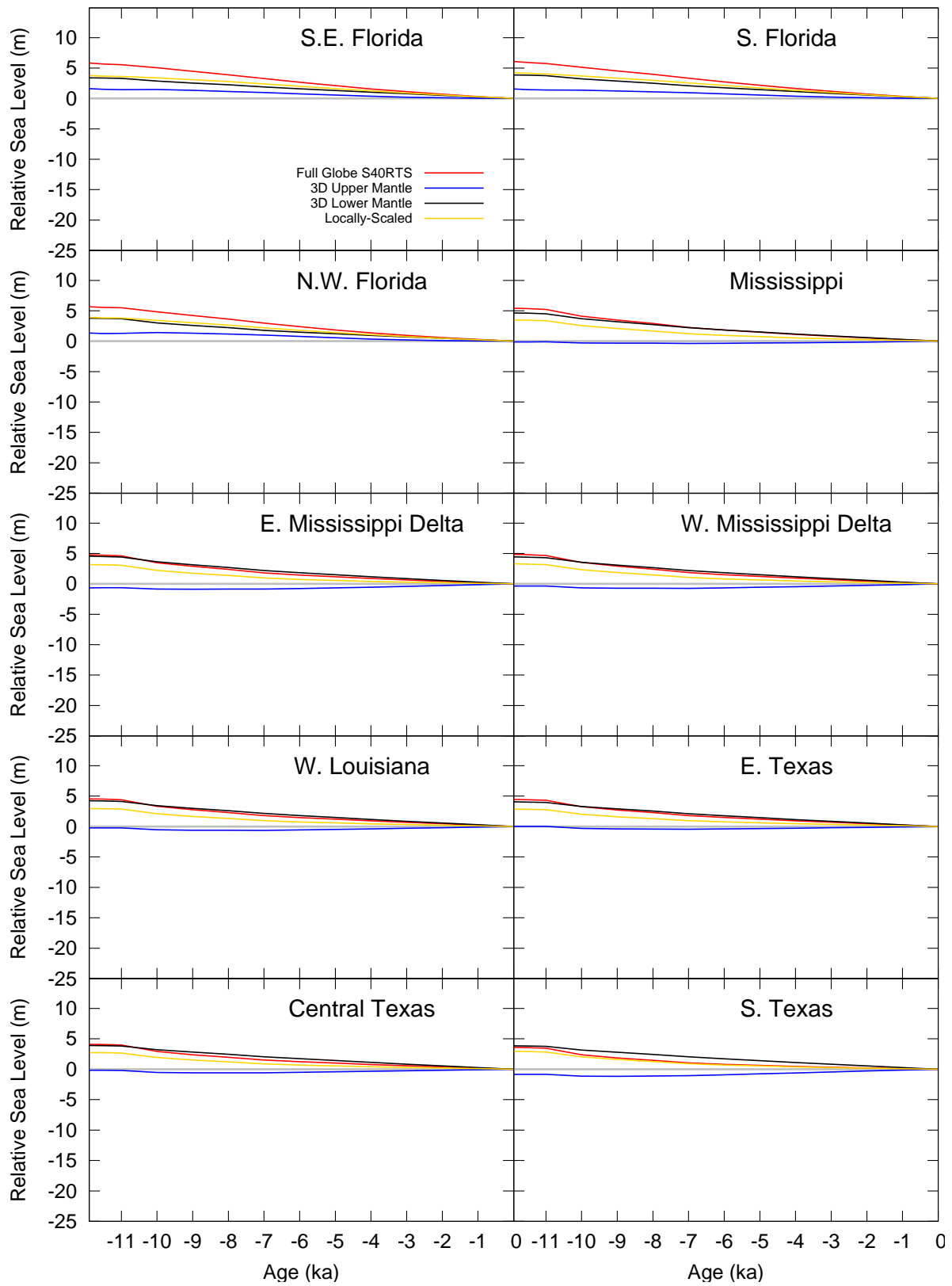


Figure S13: Continued from above.

# EARTH'S FUTURE



**Figure S13:** Continued from above.

## 5 Other Sea-Level Contributions

To provide context for the GIA contribution to future RSL estimates, we provide estimates of the contributions due to ocean steric and dynamic changes as well as that due to changes in the distribution of land ice. The methods used to define these estimates are detailed in the following sections. A summary of the results is provided in Table S2. Note that the global mean sea-level estimates are provided in the table caption. Also, the sum (right-hand-column) includes the GIA contribution provided in Table 1 ( $1\text{-}\sigma$  uncertainty ranges are those based on the compaction free SLIPs for each region).



# EARTH'S FUTURE

RCP2.6	Steric (m)		Greenland (m)		Antarctica (m)		GICs (m)		GIA (m)		Sum (m)	
St. John's, NL	0.15	[0.05-0.25]	-0.01	[-0.02-0.01]	0.06	[-0.05-0.17]	0.07	[0.05-0.09]	0.03	[0.03-0.08]	0.31	[0.07-0.58]
Halifax, NS	0.15	[0.05-0.26]	0.01	[0.00-0.01]	0.06	[-0.05-0.17]	0.07	[0.06-0.09]	0.18	[0.12-0.22]	0.47	[0.18-0.75]
Portland, ME	0.13	[0.03-0.24]	0.01	[0.01-0.02]	0.06	[-0.05-0.17]	0.08	[0.06-0.09]	0.04	[0.01-0.17]	0.33	[0.06-0.69]
Boston, MA	0.13	[0.03-0.24]	0.02	[0.01-0.03]	0.06	[-0.05-0.17]	0.08	[0.06-0.10]	0.09	[0.05-0.21]	0.38	[0.10-0.74]
New York, NY	0.10	[-0.01-0.20]	0.02	[0.01-0.04]	0.06	[-0.05-0.17]	0.08	[0.06-0.10]	0.12	[0.09-0.21]	0.38	[0.11-0.72]
Washington, DC	0.13	[0.04-0.21]	0.03	[0.02-0.05]	0.06	[-0.05-0.17]	0.08	[0.06-0.10]	0.12	[0.10-0.17]	0.42	[0.17-0.70]
Virginia Beach, VA	0.13	[0.06-0.21]	0.03	[0.02-0.05]	0.06	[-0.05-0.17]	0.09	[0.07-0.11]	0.10	[0.07-0.14]	0.41	[0.17-0.69]
Charleston, SC	0.13	[0.07-0.19]	0.04	[0.02-0.07]	0.06	[-0.05-0.17]	0.09	[0.07-0.11]	0.06	[0.03-0.06]	0.38	[0.14-0.61]
Daytona Beach, FL	0.13	[0.08-0.19]	0.04	[0.03-0.07]	0.06	[-0.05-0.17]	0.10	[0.07-0.12]	0.03	[0.00-0.13]	0.37	[0.13-0.68]
Miami, FL	0.13	[0.08-0.19]	0.05	[0.03-0.08]	0.06	[-0.05-0.17]	0.10	[0.08-0.12]	0.03	[-0.01-0.09]	0.37	[0.13-0.65]
Tampa Bay, FL	0.13	[0.07-0.19]	0.04	[0.03-0.08]	0.06	[-0.05-0.17]	0.10	[0.07-0.12]	0.03	[0.00-0.11]	0.37	[0.13-0.67]
Panama City, FL	0.13	[0.08-0.18]	0.04	[0.03-0.07]	0.06	[-0.05-0.17]	0.09	[0.07-0.12]	0.03	[0.01-0.13]	0.36	[0.14-0.68]
New Orleans, LA *	0.13	[0.08-0.19]	0.04	[0.03-0.08]	0.06	[-0.05-0.17]	0.09	[0.07-0.12]	0.03	[0.00-0.12]	0.36	[0.14-0.67]
Galveston, TX	0.13	[0.08-0.19]	0.05	[0.03-0.08]	0.07	[-0.05-0.17]	0.09	[0.07-0.12]	0.03	[0.00-0.11]	0.37	[0.13-0.67]
GMSL	0.12	[0.08-0.17]	0.06	[0.04-0.10]	0.05	[-0.04-0.13]	0.10	[0.08-0.13]	0.00	[0.00-0.00]	0.34	[0.16-0.53]
RCP4.5	Steric (m)		Greenland (m)		Antarctica (m)		GICs (m)		GIA (m)		Sum (m)	
St. John's, NL	0.22	[0.12-0.32]	-0.02	[-0.03-0.01]	0.06	[-0.06-0.17]	0.07	[0.05-0.09]	0.03	[0.03-0.08]	0.37	[0.12-0.65]
Halifax, NS	0.22	[0.12-0.33]	0.01	[0.00-0.01]	0.06	[-0.06-0.17]	0.07	[0.05-0.10]	0.18	[0.12-0.22]	0.55	[0.23-0.83]
Portland, ME	0.22	[0.11-0.32]	0.02	[0.01-0.03]	0.06	[-0.06-0.16]	0.08	[0.05-0.10]	0.04	[0.01-0.17]	0.41	[0.13-0.78]
Boston, MA	0.21	[0.11-0.32]	0.02	[0.01-0.04]	0.06	[-0.06-0.16]	0.08	[0.06-0.10]	0.09	[0.05-0.21]	0.46	[0.17-0.82]
New York, NY	0.19	[0.09-0.30]	0.03	[0.02-0.05]	0.06	[-0.06-0.16]	0.08	[0.06-0.10]	0.12	[0.09-0.21]	0.49	[0.20-0.82]
Washington, DC	0.20	[0.11-0.28]	0.04	[0.02-0.06]	0.06	[-0.06-0.16]	0.08	[0.06-0.11]	0.12	[0.10-0.17]	0.50	[0.23-0.78]
Virginia Beach, VA	0.20	[0.11-0.28]	0.04	[0.02-0.07]	0.06	[-0.06-0.17]	0.09	[0.06-0.11]	0.10	[0.07-0.14]	0.48	[0.21-0.76]
Charleston, SC	0.17	[0.12-0.23]	0.05	[0.03-0.08]	0.06	[-0.06-0.17]	0.09	[0.07-0.12]	0.06	[0.03-0.06]	0.44	[0.18-0.66]
Daytona Beach, FL	0.18	[0.12-0.24]	0.06	[0.03-0.09]	0.06	[-0.06-0.17]	0.11	[0.08-0.14]	0.03	[0.00-0.13]	0.44	[0.18-0.76]
Miami, FL	0.18	[0.13-0.24]	0.06	[0.03-0.10]	0.06	[-0.06-0.17]	0.12	[0.09-0.14]	0.03	[-0.01-0.09]	0.45	[0.18-0.74]
Tampa Bay, FL	0.18	[0.12-0.24]	0.06	[0.03-0.10]	0.06	[-0.06-0.17]	0.11	[0.09-0.14]	0.03	[0.00-0.11]	0.45	[0.18-0.75]
Panama City, FL	0.17	[0.12-0.23]	0.06	[0.03-0.09]	0.06	[-0.06-0.16]	0.11	[0.08-0.14]	0.03	[0.01-0.13]	0.44	[0.18-0.75]
New Orleans, LA*	0.17	[0.11-0.23]	0.06	[0.03-0.10]	0.06	[-0.06-0.16]	0.11	[0.08-0.14]	0.03	[0.00-0.12]	0.43	[0.17-0.75]
Galveston, TX	0.17	[0.11-0.23]	0.06	[0.03-0.10]	0.07	[-0.06-0.16]	0.11	[0.08-0.14]	0.03	[0.00-0.11]	0.44	[0.17-0.74]
GMSL	0.17	[0.13-0.21]	0.08	[0.04-0.13]	0.05	[-0.05-0.13]	0.12	[0.09-0.15]	0.00	[0.00-0.00]	0.42	[0.21-0.62]
RCP8.5	Steric (m)		Greenland (m)		Antarctica (m)		GICs (m)		GIA (m)		Sum (m)	
St. John's, NL	0.40	[0.29-0.52]	-0.03	[-0.05-0.02]	0.05	[-0.08-0.15]	0.07	[0.05-0.09]	0.03	[0.03-0.08]	0.53	[0.24-0.83]
Halifax, NS	0.34	[0.21-0.48]	0.01	[0.01-0.02]	0.05	[-0.08-0.15]	0.07	[0.05-0.10]	0.18	[0.12-0.22]	0.66	[0.30-0.97]
Portland, ME	0.35	[0.22-0.49]	0.03	[0.02-0.05]	0.05	[-0.08-0.15]	0.08	[0.05-0.10]	0.04	[0.01-0.17]	0.55	[0.21-0.95]
Boston, MA	0.36	[0.23-0.48]	0.03	[0.02-0.06]	0.05	[-0.08-0.15]	0.08	[0.05-0.10]	0.09	[0.05-0.21]	0.60	[0.28-1.00]
New York, NY	0.34	[0.21-0.48]	0.04	[0.03-0.08]	0.05	[-0.08-0.15]	0.08	[0.06-0.11]	0.12	[0.09-0.21]	0.64	[0.30-1.03]
Washington, DC	0.34	[0.20-0.49]	0.05	[0.03-0.10]	0.05	[-0.08-0.15]	0.08	[0.06-0.11]	0.12	[0.10-0.17]	0.65	[0.30-1.02]
Virginia Beach, VA	0.32	[0.21-0.43]	0.06	[0.04-0.11]	0.05	[-0.08-0.15]	0.09	[0.06-0.12]	0.10	[0.07-0.14]	0.62	[0.30-0.95]
Charleston, SC	0.28	[0.19-0.38]	0.07	[0.05-0.14]	0.05	[-0.08-0.15]	0.09	[0.06-0.12]	0.06	[0.03-0.06]	0.56	[0.24-0.86]
Daytona Beach, FL	0.27	[0.19-0.36]	0.08	[0.05-0.16]	0.05	[-0.08-0.15]	0.14	[0.11-0.17]	0.03	[0.00-0.13]	0.58	[0.27-0.97]
Miami, FL	0.28	[0.20-0.37]	0.09	[0.06-0.17]	0.05	[-0.08-0.15]	0.15	[0.12-0.18]	0.03	[-0.01-0.09]	0.60	[0.28-0.96]
Tampa Bay, FL	0.27	[0.19-0.36]	0.09	[0.05-0.16]	0.05	[-0.08-0.15]	0.15	[0.11-0.18]	0.03	[0.00-0.11]	0.59	[0.27-0.96]
Panama City, FL	0.27	[0.19-0.34]	0.09	[0.05-0.16]	0.05	[-0.08-0.15]	0.14	[0.11-0.17]	0.03	[0.01-0.13]	0.58	[0.28-0.96]
New Orleans, LA*	0.25	[0.15-0.36]	0.09	[0.05-0.16]	0.05	[-0.08-0.15]	0.14	[0.11-0.17]	0.03	[0.00-0.12]	0.56	[0.23-0.97]
Galveston, TX	0.27	[0.19-0.34]	0.09	[0.06-0.17]	0.05	[-0.08-0.15]	0.14	[0.11-0.17]	0.03	[0.00-0.11]	0.58	[0.28-0.95]
GMSL	0.26	[0.21-0.32]	0.12	[0.07-0.22]	0.04	[-0.06-0.12]	0.16	[0.03-0.12]	0.00	[0.00-0.00]	0.58	[0.34-0.84]

**Table S2:** Sea level projection data for each of the representative concentration pathway (RCP) scenarios for several major cities along the East and Gulf coasts of North America. Methods used are described in the relevant sections of the main text and in the sections below. Here we show the median values for the period 2085-2100 relative to 2006-2015 as well as the estimated 1- $\sigma$  range from the model output considered. The uncertainty range in the sum (right-hand column) was determined by simply adding the uncertainty ranges in the individual components and so is a conservative estimate of the total 1- $\sigma$  uncertainty. For Antarctica and Greenland, median values were obtained from *Church et al.* (2013); see Supplemental Material Section 7. Note the range for the GIA contribution is that based on the compaction free SLIPs using the more heuristic approach described in the main text. The results for RCP6.0 are not included as they are very similar to those for RCP4.5. Note that while GIA does result in a global mean change in sea-surface height (*Mitrovica and Milne* (2002)), it does not contribute to a global mean change in RSL (or, equivalently, ocean water volume). The acronym GICs represents ‘glaciers and ice caps’.

\*The contribution from land subsidence due to artificial drainage and sediment compaction/loading, which are significant for this locality, are not included in the values given.

Location	Rate [1- $\sigma$ CF] [1- $\sigma$ all] (mm/a)			RSL (GIA) [1- $\sigma$ CF] [1- $\sigma$ all] (m)			RSL (RCP4.5)[1- $\sigma$ ] (m)
St. John's, NL	0.43	[-0.20-2.67]	[-0.38-2.67]	0.03	[-0.02-0.22]	[-0.03-0.22]	0.37 [0.12-0.65]
Halifax, NS	2.14	[1.49-2.58]	[1.46-2.60]	0.18	[0.12-0.21]	[0.12-0.21]	0.55 [0.23-0.83]
Portland, ME	0.51	[0.49-0.72]	[0.32-0.91]	0.04	[0.04-0.06]	[0.03-0.07]	0.41 [0.13-0.78]
Boston, MA	1.06	[0.87-1.18]	[0.81-1.28]	0.09	[0.07-0.10]	[0.07-0.10]	0.46 [0.17-0.82]
New York, NY	1.44	[1.06-1.91]	[1.16-1.67]	0.12	[0.09-0.16]	[0.09-0.14]	0.49 [0.20-0.82]
Washington, DC	1.45	[1.31-1.78]	[1.26-1.75]	0.12	[0.11-0.15]	[0.10-0.14]	0.50 [0.23-0.78]
Virginia Beach, VA	1.17	[0.94-1.42]	[0.94-1.45]	0.10	[0.08-0.12]	[0.08-0.12]	0.48 [0.21-0.76]
Charleston, SC	0.70	[0.29-0.99]	[0.33-0.99]	0.06	[0.02-0.08]	[0.03-0.08]	0.44 [0.18-0.66]
Daytona Beach, FL	0.37	[0.18-0.56]	[0.17-0.59]	0.03	[0.01-0.05]	[0.01-0.05]	0.44 [0.18-0.76]
Miami, FL	0.35	[0.03-0.50]	[0.03-0.51]	0.03	[0.00-0.04]	[0.00-0.04]	0.45 [0.18-0.74]
Tampa Bay, FL	0.35	[0.12-0.51]	[0.12-0.53]	0.03	[0.01-0.04]	[0.01-0.04]	0.45 [0.18-0.75]
Panama City, FL	0.37	[0.19-0.57]	[0.17-0.52]	0.03	[0.02-0.05]	[0.01-0.04]	0.44 [0.18-0.75]
New Orleans, LA	0.32	[0.16-0.48]	[0.16-0.41]	0.03	[0.01-0.04]	[0.01-0.03]	0.43 [0.17-0.75]
Galveston, TX	0.35	[0.19-0.40]	[0.19-0.44]	0.03	[0.02-0.03]	[0.02-0.04]	0.44 [0.17-0.74]

**Table S3:** Estimated future contribution of GIA to RSL for 13 major cities along the Atlantic and Gulf coasts of North America generated using the spherically symmetric Earth model. The projections are defined as a rate for user convenience. The best-estimate values for each city are based on the parameter vector that minimized the misfit criterion for each of the three geographic regions defined in the main text. The bounds are constructed following the nominally Bayesian approach defined in the main text. Results using the more heuristic approach are given in Table 1. For context, the final column shows RSL projections that include GIA and the processes described in Section 3 for one of the intermediate climate forcing scenarios considered (Representative Concentration Pathway (RCP) 4.5).

## 6 Steric Sea-Level Change

Although the CMIP5 project has outlined numerous standards that model output should adhere to, the results of each group often require post processing to various degrees. The issue most commonly encountered is the use of a non-uniformly spaced and non-regular grid upon which the relevant physics are modelled. To deal with these differences, the end user is required to perform co-ordinate transformations from one grid to another. Post-processing is also required to correct for model drift, discussed below.

The CMIP5 project prescribes three primary data output fields that participating modelling groups should provide as appropriate, ZOS, ZOSGA, and ZOSTOGA, which represent, respectively, sea-surface height above the geoid (due to dynamical effects) and global average sea level (from all processes), and global average sea level due to thermosteric effects only. ZOS is a field prescribed for all ocean surfaces on the Earth and is a function of time, in contrast ZOSGA and ZOSTOGA are only a function of time. In addition, not all groups needed to provide both ZOSTOGA and ZOSGA, they needed to do so only in the case that they differed. We preferentially utilized the ZOSTOGA output and used ZOSGA only when ZOSTOGA was not reported by modelling groups. As previously mentioned, multiple models utilize non-regular model grids and so in order to apply common post processing methods to all model output, we resampled the output onto the same grid through spatial resampling routines. Model drift refers to a long term progression away from the steady state condition that AOGCMs are vulnerable to. To correct for this, research groups participating in the CMIP5 project are required to submit a model run where there is no forcing on the system outside those of a pre-industrial climate have been imposed on the system. Sea-level output from these runs typically exhibit a linear trend which quantifies the drift in this quantity for a particular model. To remove this signal we simply fit the ZOS and ZOS(TO)GA output with a linear trend to determine the drift correction as a function of time. Another such correction that must be made is to correct the ZOS output with respect to its global average, that is we process the data such that the global mean of the ZOS data is zero at all times. The area-weighted global mean of ZOS data output should have been corrected to zero by each modelling group prior to uploading data to the CMIP5 archive. However, we have found that not all groups performed this step and so this value is calculated in the procedure applied here to ensure that all output is consistent in this respect. To summarise, in order to make a projection of sea level utilizing the climate data we use:

$$\Delta SL^{R,M}(\theta, \phi, t) = \overline{SL_{ZOS}^{R,M}(\theta, \phi, t)} - \overline{SL_{ZOS}^{R,M}(\theta, \phi, t_0)} + \frac{\overline{SL_{ZOS(TO)GA}^{R,M}(t)} - \overline{SL_{ZOS(TO)GA}^{R,M}(t_0)} - \overline{\Delta SL_{drift}^{R,M}(\theta, \phi, t)}}{1} \quad (4)$$

where  $\theta, \phi$  are the usual spherical co-ordinates,  $t$  is the time period of interest(2085-2100),  $t_0$  is the initial reference time period the projection is made relative to (2006-2015),  $R$  denotes the RCP scenario used and  $M$  denotes the AOGCM. The overbars indicate that we adopt time averages of the model output for the respective time periods. This is done to remove any bias associated with short-term fluctuations in model output. The last term, which corrects for model drift, is given by

$$\Delta SL_{drift}^{R,M}(\theta, \phi, t) = \left( D_{ZOS}^{control,M}(\theta, \phi) + D_{ZOS(TO)GA}^{control,M} \right) (t - t_0), \quad (5)$$

where  $D_{ZOS}$  and  $D_{ZOS(TO)GA}$  are the rates determined by fitting linear trends to the pre-industrial control run output. The uncertainty for the contribution of the steric effect is determined by taking the standard deviation of the sea-level projections at each location. The data used to calculate the steric component does not extend to the shorelines due to the coarse nature of the AOGCMs, this is alleviated through the use of a nearest-neighbor interpolation method.

Fig. S14 shows some model time series for St. John's, Newfoundland. SM Table S4 lists the data providers and model names from which output was used in this analysis. SM Table S5 details which output was considered for each future climate scenario. The choice of models was primarily governed by what data was available from the PCMDI node of the ESGF as at the time this work was done. It

was not apparent that each of the ESGF nodes did not list all available data at each of the nodes (as a result of this problem, the resource was shut-down and rebuilt for over a year). Each of the runs used in this study were from the r1i1p1 realization and only one realization from each model was chosen so as to not give greater precedence to any single model. We note that this subset of models is smaller than that presently available in the CMIP5 archives, unfortunately this dataset was extracted shortly before the archive was taken down for restructuring due to fundamental technical issues and thus we were unable to extract a larger subset over the development of this study.

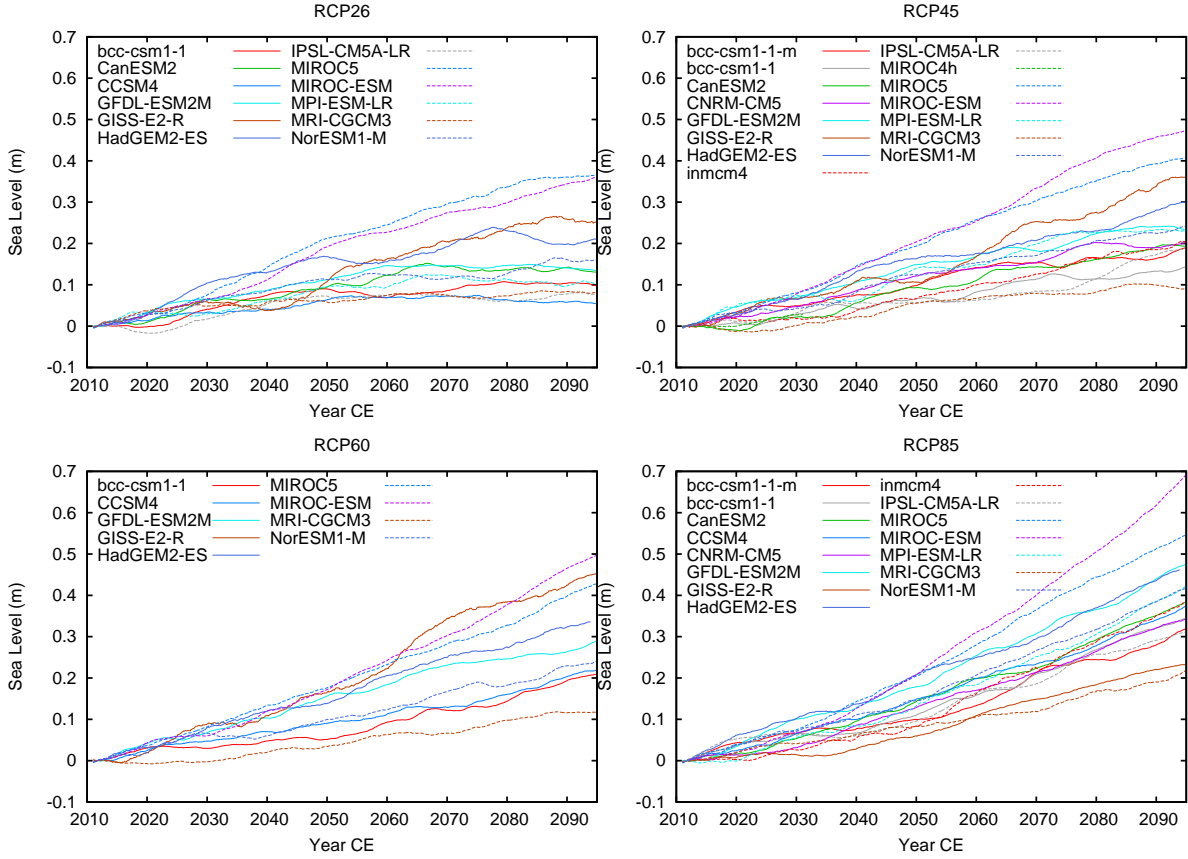


**Figure S14:** Time series (10-year running mean) for St. John's Newfoundland for all RCP scenarios. While the climate model results typically agree on the sign of sea-level change they can significantly disagree in the magnitude.

Climate Research Center	Climate Model Name
Beijing Climate Center, China Meteorological Administration	BCC-CSM1-1 BCC-CSM1-1-M
Canadian Centre for Climate Modelling and Analysis	CanESM2
National Center for Atmospheric Research	CCSM4
Centre National de Recherches Météorologiques/ Centre Européen de Recherche et Formation Avancée en Calcul Scientifique	CNRM-CM5
NOAA Geophysical Fluid Dynamics Laboratory	GFDL-ESM2M
NASA Goddard Institute for Space Studies	GISS-E2-R
Met Office Hadley Centre(additional HadGEM2-ES realizations contributed by Instituto Nacional de Pesquisas Espaciais)	HadGEM2-ES
Institute for Numerical Mathematics	INM-CM4
Institut Pierre-Simon Laplace	IPSL-CM5A-LR
Japan Agency for Marine-Earth Science and Technology, Atmo- sphere and Ocean Research Institute (The University of Tokyo), and National Institute for Environmental Studies	MIROC-ESM MIROC5
Max-Planck-Institut für Meteorologie (Max Planck Institute for Meteorology)	MPI-ESM-LR
Meteorological Research Institute	MRI-CGCM3

**Table S4:** Providers and model names for the climate model output used in this work. Not every model was run for every RCP scenario but there is at least one RCP forced run to 2100CE. On average each model provides data for  $\approx 3$  of 4 RCP scenarios.

RCP2.6	RCP4.5	RCP6.0	RCP8.5
BCC-CSM1-1	BCC-CSM1-1	BCC-CSM1-1	
CanESM2	CanESM2		CanESM2
	CNRM-CM5		CNRM-CM5
GISS-E2-R	GISS-E2-R	GISS-E2-R	GISS-E2-R
HadGEM2-ES	HadGEM2-ES	HadGEM2-ES	HadGEM2-ES
	INMCM4		INMCM4
IPSL-CM5A-LR	IPSL-CM5A-LR	IPSL-CM5A-LR	IPSL-CM5A-LR
MIROC5	MIROC5	MIROC5	MIROC5
MIROC-ESM	MIROC-ESM	MIROC-ESM	MIROC-ESM
MPI-ESM-LR	MPI-ESM-LR		MPI-ESM-LR
MRI-CGCM3	MRI-CGCM3	MRI-CGCM3	MRI-CGCM3
NorESM1-M	NorESM1-M	NorESM1-M	NorESM1-M

**Table S5:** List of which model outputs were used for each RCP projection in this study. Where possible, all of the available model output was utilised; however, some model output was not available at the time this work was done, hence the gaps in the table.

## 7 Sea-Level Change due to Mass Changes of Greenland and Antarctica

Each Gravity and Climate Experiment (GRACE) processing centre uses the same raw data but applies different processing techniques to isolate the relevant geophysical signals. As a consequence, there can be significant differences between products representing the same region, period and process. We considered products from all three processing centres when computing sea-level fingerprints.

In order to obtain sea-level fingerprints, it was first necessary to convert the gridded GRACE data sets into a usable input format for our model of sea level. This conversion was accomplished by calculating the slope of a linear fit to the time series for each grid point over the period 2006-2014 CE. If the spatial pattern in this rate was consistent between each processing centre, an average was taken for each grid point. For Greenland we used the results from all three processing centres. For Antarctica, we omitted the results from JPL given the relatively large differences between the results from this centre and the other two. The average rate of change for each point was then used as the input to the sea-level code to generate sea-level fingerprints. Since the resultant sea-level predictions are normalized by the eustatic sea-level value, they can be easily scaled to produce projections for a specified melt amplitude. The magnitude of melt has been scaled such that the resultant rate of eustatic sea-level rise is 1 mm/a, which is consistent with similar studies such as *Mitrovica et al.* (2011). To determine the uncertainty of the contributions of Greenland and Antarctica for a particular location we multiply the confidence range in the global mean sea-level value provided by *Church et al.* (2013) by the relevant fingerprint value.

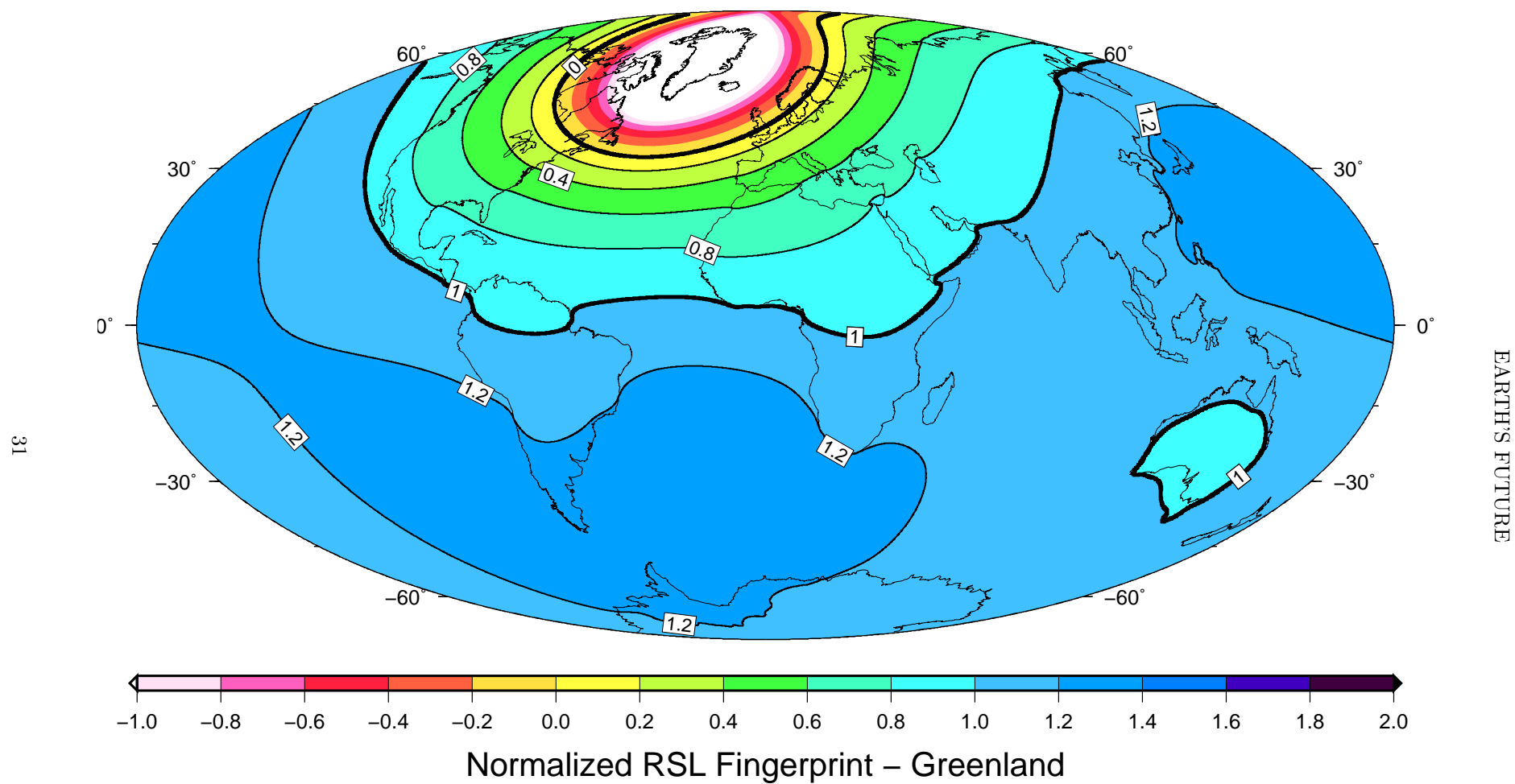
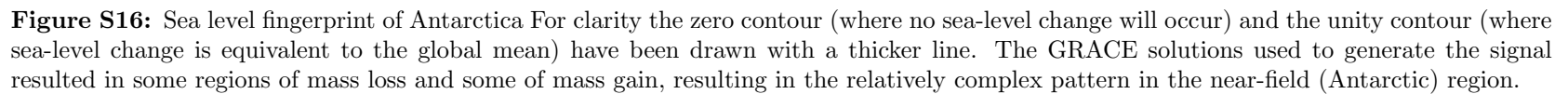


**Figure S15:** Sea level fingerprint for Greenland. This fingerprint was generated using all the GRACE products. For clarity the zero contour (where no sea-level change will occur) and the unity contour (where sea-level change is equivalent to the global mean) have been drawn with a thicker line.





## 8 Sea-Level Change due to Mass Changes of Glaciers and Ice Caps

We follow the methods adopted in *Radić and Hock* (2010) and *Huss and Farinotti* (2012) to approximate glacier volumes via statistical up-scaling from known glacier volumes. In this study we utilize the area to mean thickness scaling coefficients of *Huss and Farinotti* (2012) along with the glacier outlines of *Arendt et al.* (2014). *Huss and Farinotti* (2012) use a relationship between area and average thickness

$$\bar{h} = cS^\gamma, \quad (6)$$

where  $\bar{h}$  is the mean glacier thickness,  $c, \gamma$  are scaling coefficients and  $S$  is the glacier area. The study of *Huss and Farinotti* (2012) provides scaling coefficients for each of the 19 regions in the Randolph Glacier Inventory (RGI), typical values for  $c$  are between  $0.3 \text{ m}^{1-2\gamma}$  and  $0.6 \text{ m}^{1-2\gamma}$  and typical values for  $\gamma$  are between 0.25 and 0.35. Using these values and determining volume from them we can then use the values as input to the sea-level fingerprinting model applied to ice sheets as above. To use the glacier volumes as input loads to our model we sum up the volumes of the glaciers for each region in the RGI and bin them at the required resolution for input to our sea-level model (which was run at a spherical harmonic truncation of degree and order 1024). Some example fingerprints demonstrating the gravitational effects on sea level for various sample regions are shown in Figures S17 to S19.

In order to determine the contribution of the glaciers to changes in sea level, we require information regarding their rates of mass loss, for which we adopt the results of *Marzeion et al.* (2012). In their study they utilize climate model output (CMIP5) to drive a surface mass balance model of GICs. They provide information regarding the melt volume of GICs as a function of location (region in the RGI), time, climate model and RCP scenario. We use this information in combination with the (normalized) sea-level fingerprints (eg. Figures S17 to S19) to determine the sea-level rise for each glacier region in the RGI as a function of time, climate model, RCP scenario, latitude and longitude.

Determining the uncertainty of the GIC contribution involves several straightforward steps. First, we determine the mean variance for our two time intervals (2100-2085CE and 2015-2006CE) for each combination of RCP, climate model and RGI region and sum these together. We then scale these values by the fingerprints and sum them accordingly to determine the uncertainty for the total of each combination of RCP and climate model. Finally, to obtain the uncertainty for a given RCP scenario we simply determine the mean of the variance across all climate model forcings for a given RCP scenario and add to this the variance of the mean of the GIC contribution so as to capture both the uncertainty provided by *Marzeion et al.* (2012) and the spread in the GIC contribution.

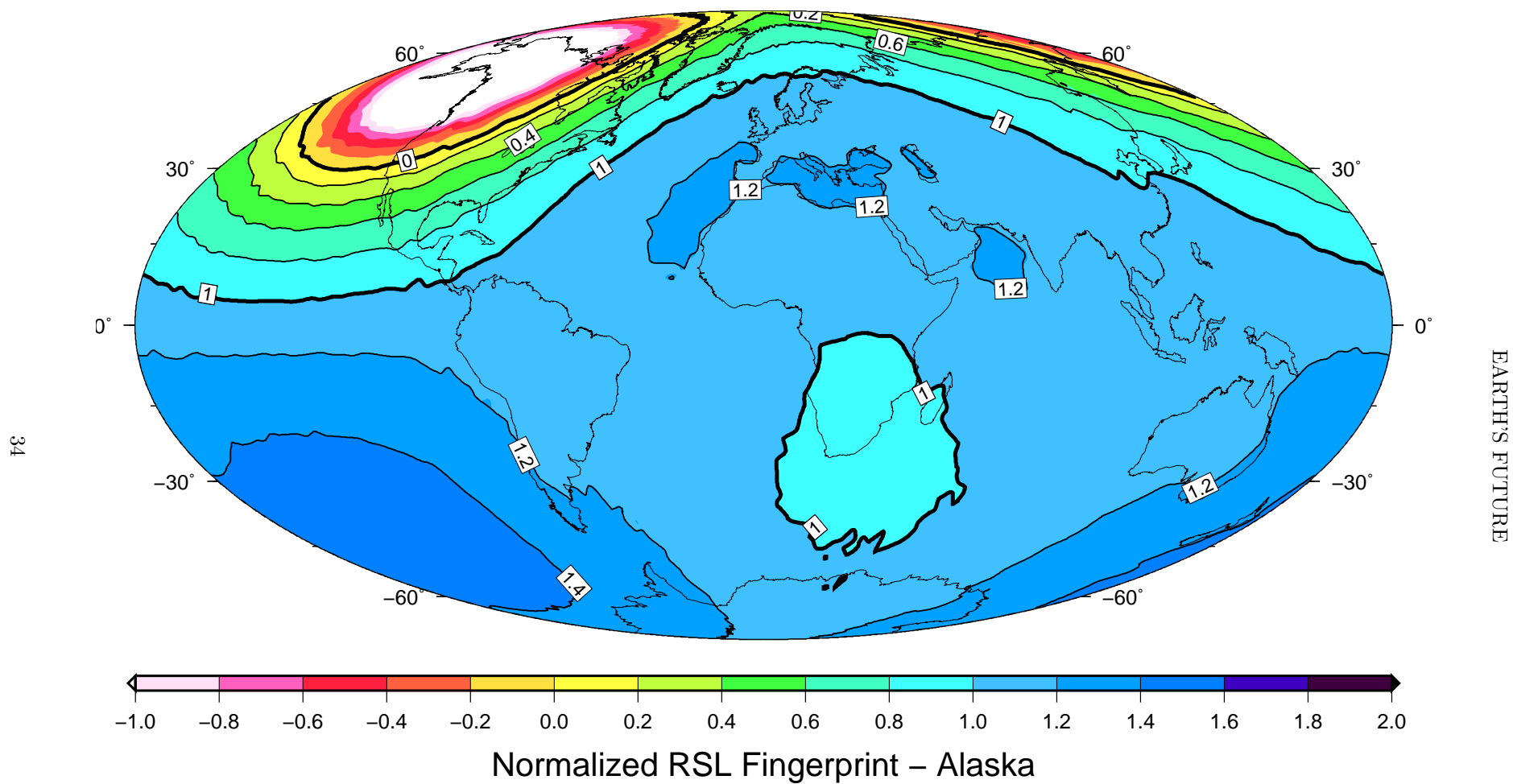


**Figure S17:** Sea level fingerprint of the GICs of Alaska. The fingerprint is a typical example of a near-field signal (when comparing to our regions of interest). Note some spatial filtering has been applied as these signals are somewhat more sensitive to noise than those fingerprints in Figures S16 and S15.

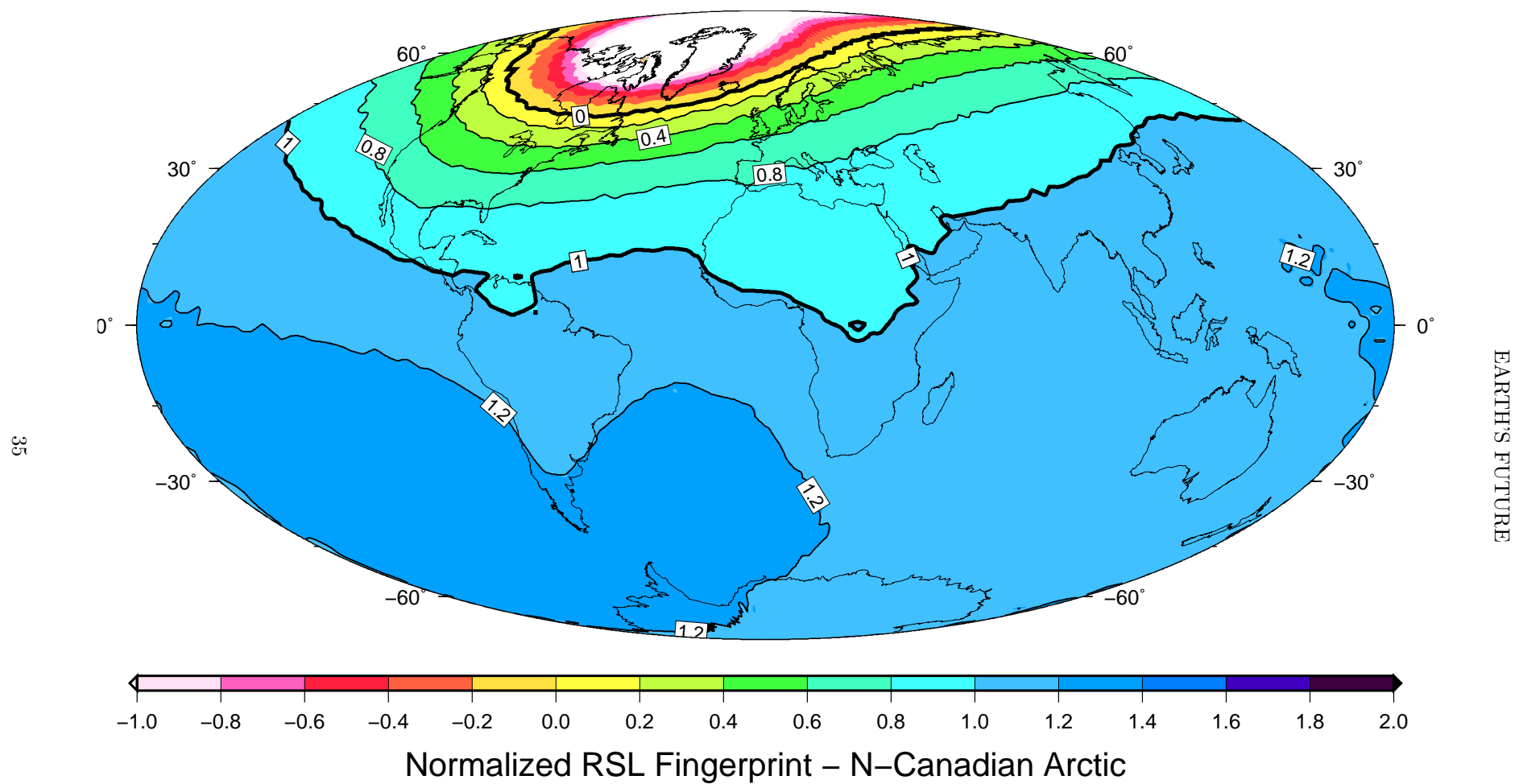


**Figure S18:** Sea level fingerprint of the GICs of the Northern Canadian Arctic. The fingerprint is a typical example of a near-field signal (when comparing to our regions of interest). Note some spatial filtering has been applied as these signals are somewhat more sensitive to noise than those fingerprints in Figures S16 and S15.

